Generalized Linear Quaternion Complementary Filter for Attitude Estimation from Multi-Sensor Observations: An Optimization Approach

Article *in* IEEE Transactions on Automation Science and Engineering · July 2019

DOI: 10.1109/TASE.2018.2888908

CITATIONS
46

READS
1,518

5 authors, including:

Jin Wu
The Hong Kong University of Science and Technology
102 PUBLICATIONS **603** CITATIONS
SEE PROFILE

Zebo Zhou
University of Electronic Science and Technology of China
55 PUBLICATIONS **709** CITATIONS
SEE PROFILE

Hassen Fourati
University of Grenoble
91 PUBLICATIONS **1,092** CITATIONS
SEE PROFILE

R. Li
University of Electronic Science and Technology of China
51 PUBLICATIONS **599** CITATIONS
SEE PROFILE

Generalized Linear Quaternion Complementary Filter for Attitude Estimation From Multisensor Observations: An Optimization Approach

Jin Wu, *Member, IEEE*, Zebo Zhou, Hassen Fourati, Rui Li, *Member, IEEE*, and Ming Liu, *Senior Member, IEEE*

***Abstract*— Focusing on generalized sensor combinations, this paper deals with the attitude estimation problem using a linear complementary filter (CF). The quaternion observation model is obtained via a gradient descent algorithm. An additive measurement model is then established according to derived results. The filter is named as the generalized CF where the observation model is simplified as a linear one that is quite different from previous-reported brute-force nonlinear results. Moreover, we prove that representative derivative-based optimization algorithms are essentially equivalent to each other. Derivations are given to establish the state model based on the quaternion kinematic equation. The proposed algorithm is validated under several experimental conditions involving the free-living environment, harsh external field disturbances, and aerial flight test aided by robotic vision. Using the specially designed experimental devices, data acquisition and algorithm computations are performed to give comparisons on accuracy, robustness, time-consumption, and so on with representative methods. The results show that not only the proposed filter can give fast, accurate, and stable estimates in terms of various sensor combinations but also produces robust attitude estimation in the scenario of harsh situations, e.g., irregular magnetic distortion.**

***Note to Practitioners*—Multisensor attitude estimation is a crucial technique in robotic devices. Many existing methods focus on the orientation fusion of specific sensor combinations. In this paper, we make the problem more concise. The results given in this paper are very general and can significantly decrease the space consumption and computation burden without losing the original estimation accuracy. Such performance will be of benefit to robotic platforms requiring flexible and easy-to-tune attitude estimation in the future.**

***Index Terms*— Attitude estimation, complementary filter, multisensor fusion, quaternion optimization, robotics.**

Manuscript received August 4, 2018; accepted December 13, 2018. Date of publication January 9, 2019; date of current version July 1, 2019. This paper was recommended for publication by Associate Editor H. Liu and Editor D. Popa upon evaluation of the reviewers' comments. This work was supported in part by the National Natural Science Foundation of China under Grant 41604025 and Grant 61450010, in part by the State Key Laboratory of Geodesy and Earth's Dynamics, Institute of Geodesy and Geophysics, CAS, under Grant SKLGED2018-3-2-E, and in part by the Fundamental Research Funds for the Central Universities under Grant ZYGX2018J080. *(Corresponding author: Zebo Zhou.)*

J. Wu and Z. Zhou are with the School of Aeronautics and Astronautics, University of Electronic Science and Technology of China, Chengdu 610054, China, and also with the State Key Laboratory of Geodesy and Earth's Dynamics, Institute of Geodesy and Geophysics, Chinese Academy of Sciences, Beijing 100864, China (e-mail: jin_wu_uestc@hotmail.com; klinsmann.zhou@gmail.com).

H. Fourati is with the GIPSA-Lab, CNRS, University Grenoble Alpes, Grenoble 38400, France, and also with Inria, 78153 Le Chesnay, France (e-mail: hassen.fourati@gipsa-lab.grenoble-inp.fr).

R. Li is with the School of Automation, University of Electronic Science and Technology of China, Chengdu 610054, China (e-mail: hitlirui@gmail.com).

M. Liu is with the Department of Electronic and Computer Engineering, Hong Kong University of Science and Technology, Hong Kong (e-mail: eelium@ust.hk).

Color versions of one or more of the figures in this paper are available online at http://ieeexplore.ieee.org.

Digital Object Identifier 10.1109/TASE.2018.2888908

I. Introduction

THE development of consumer electronics brings a worldwide mania in cell phones, smart wearables, interactive devices, and so on [1]–[3]. Such electronic products indeed improve the quality of our living. As a matter of fact, each product is a mixture of many recent technological advances. Among all these techniques, the sensor fusion is of importance since it gives state estimation of the body's motion from multisensor observations [4]–[6]. Attitude estimation, as part of the overall sensor fusion module, plays a big role in detecting object's attitude and further produces signals for gait analysis and gravity sensing [7], [8]. The attitude estimation techniques will provide key bases for later robotic estimation and planning [9].

Not only consumer electronics but many other professional applications also have increasing demands on attitude estimation [10], [11]. For instance, one satellite needs to be stabilized on the orbit and to achieve this, the attitude estimator should give accurate estimates for the control tasks [12]. Moreover, such applications can also be operated under harsh external conditions, i.e., strong vibration, sudden external acceleration, irregular magnetic distortion, ventilation caused by rotors, and so on [13], [14], which make the attitude estimation more challenging [15]–[17]. In engineering practice, a navigation system should have sufficient redundant computation resources to ensure the robustness of the system when emergence happens [18]. For example, an unmanned aerial vehicle (UAV) system needs to act quickly for failsafe when some incidents take place such as motor failure, GPS outage, and main controller failure [19], [20]. This, in a degree, requires the navigation part to be computationally efficient.

In fact, Kalman filter (KF) [21] is an optimal filtering approach in the sense of minimum mean squared error. Although other filtering approaches, e.g., H_∞ filter [22], have been widely spread, KF still remains its definite coverage in industrial applications. The attitude estimation can be

efficiently achieved via KF-related algorithms [23]. However, conventional KF methods still have some drawbacks as follows.

1) Classical KF requires the state and observation models to be linear. In addition, the noise sources for the two models should be white Gaussian and uncorrelated.
2) Although many techniques have been developed to deal with nonlinearities, e.g., the extended KF [24], the unscented KF [25], and so on [26], they will significantly increase the computational burden.
3) In principle, a three-order KF can already obtain good attitude estimates [27], but for engineering requirements, some KF-based attitude estimators are designed to accommodate high-dimension observation models [15], [28] for augmented estimation, which makes the filtering time-costly.

Complementary filter (CF) approaches are popular alternatives for low-cost platforms with need of attitude estimation [29]–[32]. Associated thoughts have been proposed for many years [33]. Recent advances mainly focus on the combination of magnetic, angular rate, and gravity (MARG) sensors, i.e., the magnetometer, gyroscope, and accelerometer. Marins *et al.* [34] uses the Gauss–Newton algorithm (GNA) to obtain the quaternion solution to the accelerometer–magnetometer attitude determination. Another method using the error cross product is studied by Euston *et al.* [35] and Mahony *et al.* [36]. Madgwick *et al.* [37] give another point of view where the gradient descent algorithm (GDA) is adopted. In the similar way, Tian *et al.* [38], [39] proposed the method based on improved GNA (IGNA) while Fourati *et al.* [40], [41] use the Levenberg–Marquardt algorithm (LMA). After attitude determination from vector observations, these methods jointly employ the linear CF (LCF) as the attitude observer.

It can be seen that these advances mainly face the attitude solution from the accelerometer–magnetometer combination. In fact, this is a specific case of Wahba's problem [42], [43]. This leads to a new CF algorithm developed by Marantos *et al.* [19] which uses the singular value decomposition (SVD [44], [45]) as Wahba's solution, which compensates for the gyroscope's random drift. However, Wahba's problem will have two solutions when there is only one vector observation that makes the attitude solution ambiguous at the same time [43], [46].

All the above-mentioned methods generate efficient attitude estimation but they have some joint or respective disadvantages as follows.

1) They just focus on almost the same sensor combination, i.e., MARG sensors. Generalized sensor combinations under optimal framework are not well studied.
2) For GDA, IGNA, and LMA, brute-force use of the optimization will make the algorithms computationally expensive, i.e., some mathematical internals should be investigated further.

Inspired by the above-mentioned representative methods along with their advantages and disadvantages, this paper deals with a novel CF scheme whose main contributions are as follows.

1) Using quaternion representation, the generalized attitude estimation is solved using GDA. Various strapdown sensors such as accelerometer, magnetometer, camera, sun sensor, nadir sensor, and so on can be efficiently fused. The architecture is derived to be additive and linear, which is simple for implementation and fault detection.
2) With finding in this paper, previous derivative-based optimization methods for attitude estimation are proven to be equivalent to each other.

Experiments on robotic platforms are designed and carried out which verify the proposed filter's effectiveness and advantages compared with representative methods.

This paper has the following arrangement of contents. Section II introduces the proposed problem formulation of the generalized sensor fusion from vector observations. Section III contains the proposed GDA method for attitude determination from strapdown sensors. Section IV involves the proposed CF design including the basic structure, robustness ensurance, and some further discussions of mathematical properties. Hardware, experiments, and results are presented in Section V, showing the effectiveness of the proposed filter with respect to reference device and representative methods. Section VI gives the concluding remarks.

II. Generalized Sensor Fusion

For a multisensor combination on a rigid platform, its fusion equations can be given by

$$\begin{cases} \boldsymbol{D}_1^b = \boldsymbol{C}\boldsymbol{D}_1^r \\ \boldsymbol{D}_2^b = \boldsymbol{C}\boldsymbol{D}_2^r \\ \quad \cdots \\ \boldsymbol{D}_n^b = \boldsymbol{C}\boldsymbol{D}_n^r \end{cases} \tag{1}$$

where $\boldsymbol{D}_i^b = (D_{x,i}^b, D_{y,i}^b, D_{z,i}^b)^\top$ denotes the ith vector observation in the body frame b while $\boldsymbol{D}_i^r = (D_{x,i}^r, D_{y,i}^r, D_{z,i}^r)^\top$ denotes the ith vector observation in the reference frame r. $\boldsymbol{C}$ stands for the direction cosine matrix (DCM). The above-mentioned equation can be converted to a least-square loss function

$$\mathcal{J}(\boldsymbol{C}) = \sum_{i=1}^{n} \left\| \boldsymbol{C}\boldsymbol{D}_i^r - \boldsymbol{D}_i^b \right\|^2 \tag{2}$$

with the aim of

$$\underset{\boldsymbol{C}\boldsymbol{C}^\top = \boldsymbol{C}^\top\boldsymbol{C} = \boldsymbol{I}, \det(\boldsymbol{C}) = +1}{\arg\min} \quad \mathcal{J}(\boldsymbol{C}) \tag{3}$$

where $\boldsymbol{I}$ is the identity matrix with proper dimension and $\|\cdot\|$ is the simplification of the Euclidean norm. A possible solution for this problem using SVD is given in [44]. When the weights of various sensors are concerned, the problem will be identical to Wahba's problem [42], such that

$$\underset{\boldsymbol{C}\boldsymbol{C}^\top = \boldsymbol{C}^\top\boldsymbol{C} = \boldsymbol{I}, \det(\boldsymbol{C}) = +1}{\arg\min} \sum_{i=1}^{n} a_i \left\| \boldsymbol{C}\boldsymbol{D}_i^r - \boldsymbol{D}_i^b \right\|^2 \tag{4}$$

where a_i denotes the positive weight of the ith sensor with the property of $\sum_{i=1}^{n} a_i = 1$. Wahba's solutions include a variety of famous algorithms, e.g., QUEST, FOAM, and SVD [45], [47], [48]. A recent fast solver FLAE maintains

the same accuracy as developed in [49]. Now, we study the fusion problem for a single sensor. The subequation of (1) can be further given by

$$\begin{aligned}\boldsymbol{D}_i^b &= \boldsymbol{C}\boldsymbol{D}_i^r = \begin{pmatrix} C_{11} & C_{12} & C_{13} \\ C_{21} & C_{22} & C_{23} \\ C_{31} & C_{32} & C_{33} \end{pmatrix} \begin{pmatrix} D_{x,i}^r \\ D_{y,i}^r \\ D_{z,i}^r \end{pmatrix} \\ &= D_{x,i}^r \begin{pmatrix} C_{11} \\ C_{21} \\ C_{31} \end{pmatrix} + D_{y,i}^r \begin{pmatrix} C_{12} \\ C_{22} \\ C_{32} \end{pmatrix} + D_{z,i}^r \begin{pmatrix} C_{13} \\ C_{23} \\ C_{33} \end{pmatrix} \\ &= D_{x,i}^r \boldsymbol{C}_1 + D_{y,i}^r \boldsymbol{C}_2 + D_{z,i}^r \boldsymbol{C}_3 \end{aligned} \tag{5}$$

where C_{ij} is the element of $\boldsymbol{C}$ in the ith row and jth column while $\boldsymbol{C}_i$ denotes the ith column of $\boldsymbol{C}$. Namely, $\boldsymbol{D}_i^b$ is the linear combination of the three columns of the DCM.

When the DCM is represented by the quaternion $\boldsymbol{q} = (q_0, q_1, q_2, q_3)^\top$, the columns can be decomposed such as [49]

$$\begin{aligned}\boldsymbol{C}_1 &= \begin{pmatrix} q_0^2 + q_1^2 - q_2^2 - q_3^3 \\ 2q_1q_2 - 2q_0q_3 \\ 2q_0q_2 + 2q_1q_3 \end{pmatrix} \\ &= \begin{pmatrix} q_0 & q_1 & -q_2 & -q_3 \\ -q_3 & q_2 & q_1 & -q_0 \\ q_2 & q_3 & q_0 & q_1 \end{pmatrix} \begin{pmatrix} q_0 \\ q_1 \\ q_2 \\ q_3 \end{pmatrix} = \boldsymbol{P}_1(\boldsymbol{q})\boldsymbol{q} \end{aligned} \tag{6}$$

$$\begin{aligned}\boldsymbol{C}_2 &= \begin{pmatrix} 2q_1q_2 + 2q_0q_3 \\ q_0^2 - q_1^2 + q_2^2 - q_3^2 \\ -2q_0q_1 + 2q_2q_3 \end{pmatrix} \\ &= \begin{pmatrix} q_3 & q_2 & q_1 & q_0 \\ q_0 & -q_1 & q_2 & -q_3 \\ -q_1 & -q_0 & q_3 & q_2 \end{pmatrix} \begin{pmatrix} q_0 \\ q_1 \\ q_2 \\ q_3 \end{pmatrix} = \boldsymbol{P}_2(\boldsymbol{q})\boldsymbol{q} \end{aligned} \tag{7}$$

$$\begin{aligned}\boldsymbol{C}_3 &= \begin{pmatrix} -2q_0q_2 + 2q_1q_3 \\ 2q_2q_3 + 2q_0q_1 \\ q_0^2 - q_1^2 - q_2^2 + q_3^2 \end{pmatrix} \\ &= \begin{pmatrix} -q_2 & q_3 & -q_0 & q_1 \\ q_1 & q_0 & q_3 & q_2 \\ q_0 & -q_1 & -q_2 & q_3 \end{pmatrix} \begin{pmatrix} q_0 \\ q_1 \\ q_2 \\ q_3 \end{pmatrix} = \boldsymbol{P}_3(\boldsymbol{q})\boldsymbol{q}. \end{aligned} \tag{8}$$

Then, (5) is further given by

$$\begin{aligned}\boldsymbol{D}_i^b &= D_{x,1}^r \boldsymbol{C}_1 + D_{y,i}^r \boldsymbol{C}_2 + D_{z,i}^r \boldsymbol{C}_3 \\ &= [D_{x,i}^r \boldsymbol{P}_1(\boldsymbol{q}) + D_{y,i}^r \boldsymbol{P}_2(\boldsymbol{q}) + D_{z,i}^r \boldsymbol{P}_3(\boldsymbol{q})]\boldsymbol{q}. \end{aligned} \tag{9}$$

With this equation, we extend the 1-D equation to (1). The fusion error function of the ith sensor is defined by

$$\boldsymbol{f}(\boldsymbol{q}, i) = \left[D_{x,i}^r \boldsymbol{P}_1(\boldsymbol{q}) + D_{y,i}^r \boldsymbol{P}_2(\boldsymbol{q}) + D_{z,i}^r \boldsymbol{P}_3(\boldsymbol{q})\right]\boldsymbol{q} - \boldsymbol{D}_i^b. \tag{10}$$

Naturally, the error function for the whole sensor combination can be given by the augmented form

$$\boldsymbol{f}(\boldsymbol{q}, \{w, v, \cdots, n\}) = \begin{pmatrix} \boldsymbol{f}(\boldsymbol{q}, w) \\ \boldsymbol{f}(\boldsymbol{q}, v) \\ \cdots \\ \boldsymbol{f}(\boldsymbol{q}, n) \end{pmatrix} \tag{11}$$

where $\{w, v, \cdots, n\}$ denotes the set of the indexes of valid sensors which has been sorted in ascending order. In terms of the weights, the corresponding error function is defined by

$$\boldsymbol{f}(\boldsymbol{q}, \{w, v, \cdots, n\}, \{a_w, a_v, \cdots, a_n\}) = \begin{pmatrix} \sqrt{a_w}\boldsymbol{f}(\boldsymbol{q}, w) \\ \sqrt{a_v}\boldsymbol{f}(\boldsymbol{q}, v) \\ \vdots \\ \sqrt{a_n}\boldsymbol{f}(\boldsymbol{q}, n) \end{pmatrix}. \tag{12}$$

In this way, the original problem in (4) can be shifted to

$$\arg\min_{\|\boldsymbol{q}\|=1} \|\boldsymbol{F}(\boldsymbol{q})\|^2 \tag{13}$$

where for simplicity, we use

$$\boldsymbol{F}(\boldsymbol{q}) = \boldsymbol{f}(\boldsymbol{q}, \{w, v, \cdots, n\}, \{a_w, a_v, \cdots, a_n\}) \tag{14}$$

to represent the error function (12). Such problem can be solved via optimization methods. Previously, we have shown that the error function is convex with respect to unit quaternion normalization [50]. In Section III, we are going to introduce a gradient-descent algorithm.

III. Proposed GDA Method

The GDA is known to be an efficient method for optimization problems [37], [38]. It requires the derivative information of the target function with respect to the variables to be solved. In this case, the state of the system is chosen as the quaternion $\boldsymbol{q}$. The implementation of the GDA can be expressed as

$$\boldsymbol{q}_{\boldsymbol{y},k} = \boldsymbol{q}_{\boldsymbol{y},k-1} - \chi_k \nabla \boldsymbol{F}(\boldsymbol{q}_{\boldsymbol{y},k-1}), \chi_k > 0 \tag{15}$$

where χ_k is the step size of the kth iteration. The gradient of the suberror function $\boldsymbol{f}(\boldsymbol{q}, i)$ can be computed by

$$\nabla \boldsymbol{f}(\boldsymbol{q}, i) = \boldsymbol{J}_i^\top \boldsymbol{f}(\boldsymbol{q}, i) \tag{16}$$

where the Jacobian matrix $\boldsymbol{J}_i$ can be calculated by

$$\boldsymbol{J}_i = \frac{\partial \boldsymbol{f}(\boldsymbol{q}, i)}{\partial \boldsymbol{q}} = D_{x,i}^r \frac{\partial \boldsymbol{C}_1}{\partial \boldsymbol{q}} + D_{y,i}^r \frac{\partial \boldsymbol{C}_2}{\partial \boldsymbol{q}} + D_{z,i}^r \frac{\partial \boldsymbol{C}_3}{\partial \boldsymbol{q}}. \tag{17}$$

The details of $\partial \boldsymbol{C}_1/\partial \boldsymbol{q}, \partial \boldsymbol{C}_2/\partial \boldsymbol{q}, \partial \boldsymbol{C}_3/\partial \boldsymbol{q}$ are

$$\begin{aligned}\frac{\partial \boldsymbol{C}_1}{\partial \boldsymbol{q}} &= \begin{pmatrix} 2q_0 & 2q_1 & -2q_2 & -2q_3 \\ -2q_3 & 2q_2 & 2q_1 & -2q_0 \\ 2q_2 & 2q_3 & 2q_0 & 2q_1 \end{pmatrix} = 2\boldsymbol{P}_1(\boldsymbol{q}) \\ \frac{\partial \boldsymbol{C}_2}{\partial \boldsymbol{q}} &= \begin{pmatrix} 2q_3 & 2q_2 & 2q_1 & 2q_0 \\ 2q_0 & -2q_1 & 2q_2 & -2q_3 \\ -2q_1 & -2q_0 & 2q_3 & 2q_2 \end{pmatrix} = 2\boldsymbol{P}_2(\boldsymbol{q}) \\ \frac{\partial \boldsymbol{C}_3}{\partial \boldsymbol{q}} &= \begin{pmatrix} -2q_2 & 2q_3 & -2q_0 & 2q_1 \\ 2q_1 & 2q_0 & 2q_3 & 2q_2 \\ 2q_0 & -2q_1 & -2q_2 & 2q_3 \end{pmatrix} = 2\boldsymbol{P}_3(\boldsymbol{q}). \end{aligned} \tag{18}$$

Consequently $\boldsymbol{J}_i$ can be written as

$$\boldsymbol{J}_i = 2[D_{x,i}^r \boldsymbol{P}_1(\boldsymbol{q}) + D_{y,i}^r \boldsymbol{P}_2(\boldsymbol{q}) + D_{z,i}^r \boldsymbol{P}_3(\boldsymbol{q})]. \tag{19}$$

Then, the overall gradient of $\boldsymbol{F}(\boldsymbol{q})$ is given by

$$\nabla \boldsymbol{F}(\boldsymbol{q}) = \boldsymbol{J}_{\{w,v,\cdots,n\}}^\top \boldsymbol{F}(\boldsymbol{q}) \tag{20}$$

where

$$\boldsymbol{J}_{\{w,v,\cdots,n\}} = \begin{pmatrix} \sqrt{a_w}\boldsymbol{J}_w \\ \sqrt{a_v}\boldsymbol{J}_v \\ \cdots \\ \sqrt{a_n}\boldsymbol{J}_n \end{pmatrix}. \tag{21}$$

Thereby, (20) can be further written as

$$\begin{aligned} \nabla \boldsymbol{F}(\boldsymbol{q}) &= \boldsymbol{J}^{\top}_{\{w,v,\cdots,n\}} \boldsymbol{F}(\boldsymbol{q}) \\ &= \left(\sqrt{a_w}\boldsymbol{J}_w^{\top}, \sqrt{a_v}\boldsymbol{J}_v^{\top}, \cdots, \sqrt{a_n}\boldsymbol{J}_n^{\top}\right) \begin{pmatrix} \sqrt{a_w}\boldsymbol{f}(\boldsymbol{q}, w) \\ \sqrt{a_v}\boldsymbol{f}(\boldsymbol{q}, v) \\ \cdots \\ \sqrt{a_n}\boldsymbol{f}(\boldsymbol{q}, n) \end{pmatrix} \\ &= \sum_{i\in\{w,v,\cdots,n\}} a_i \boldsymbol{J}_i^{\top} \boldsymbol{f}(\boldsymbol{q}, i). \end{aligned} \tag{22}$$

Letting (see the Appendix)

$$\begin{aligned} \boldsymbol{P}_1^{\top}(\boldsymbol{q})\boldsymbol{D}_i^b &= \boldsymbol{M}_1(\boldsymbol{D}_i^b)\boldsymbol{q} \\ \boldsymbol{P}_2^{\top}(\boldsymbol{q})\boldsymbol{D}_i^b &= \boldsymbol{M}_2(\boldsymbol{D}_i^b)\boldsymbol{q} \\ \boldsymbol{P}_3^{\top}(\boldsymbol{q})\boldsymbol{D}_i^b &= \boldsymbol{M}_3(\boldsymbol{D}_i^b)\boldsymbol{q} \end{aligned} \tag{23}$$

the gradient arrives at

$$\begin{aligned} \nabla \boldsymbol{F}(\boldsymbol{q}) &= \sum_{i\in\{w,v,\cdots,n\}} a_i [\frac{1}{2}\boldsymbol{J}_i^{\top}(\boldsymbol{q})\boldsymbol{J}_i(\boldsymbol{q})\boldsymbol{q} - \boldsymbol{J}_i^{\top}(\boldsymbol{q})\boldsymbol{D}_i^b] \\ &= 2 \sum_{i\in\{w,v,\cdots,n\}} a_i \begin{bmatrix} \frac{1}{4}\boldsymbol{J}_i^{\top}(\boldsymbol{q})\boldsymbol{J}_i(\boldsymbol{q}) - D^r_{x,i}\boldsymbol{M}_1(\boldsymbol{D}_i^b) \\ -D^r_{y,i}\boldsymbol{M}_2(\boldsymbol{D}_i^b) - D^r_{z,i}\boldsymbol{M}_3(\boldsymbol{D}_i^b) \end{bmatrix} \boldsymbol{q}. \end{aligned} \tag{24}$$

The operator $\boldsymbol{\Sigma}(\boldsymbol{q})$ is defined by

$$\boldsymbol{\Sigma}(\boldsymbol{q}) = \sum_{i\in\{w,v,\cdots,n\}} a_i \begin{bmatrix} \frac{1}{4}\boldsymbol{J}_i^{\top}(\boldsymbol{q})\boldsymbol{J}_i(\boldsymbol{q}) - D^r_{x,i}\boldsymbol{M}_1(\boldsymbol{D}_i^b) \\ -D^r_{y,i}\boldsymbol{M}_2(\boldsymbol{D}_i^b) - D^r_{z,i}\boldsymbol{M}_3(\boldsymbol{D}_i^b) \end{bmatrix}. \tag{25}$$

Theorem 1: The equations

$$\begin{cases} \boldsymbol{P}_1^{\top}(\boldsymbol{q})\boldsymbol{P}_1(\boldsymbol{q})\boldsymbol{q} = \boldsymbol{q} \\ \boldsymbol{P}_2^{\top}(\boldsymbol{q})\boldsymbol{P}_2(\boldsymbol{q})\boldsymbol{q} = \boldsymbol{q} \\ \boldsymbol{P}_3^{\top}(\boldsymbol{q})\boldsymbol{P}_3(\boldsymbol{q})\boldsymbol{q} = \boldsymbol{q} \end{cases} \tag{26}$$

always hold for arbitrary unit quaternion.

Proof: See the Appendix. ∎

Lemma 1: With the derivation of Theorem 1, we have the following equalities holding as well:

$$\left[\boldsymbol{P}_j^{\top}(\boldsymbol{q})\boldsymbol{P}_k(\boldsymbol{q}) + \boldsymbol{P}_k^{\top}(\boldsymbol{q})\boldsymbol{P}_j(\boldsymbol{q})\right]\boldsymbol{q} = \boldsymbol{0}_{4\times 1} \tag{27}$$

where the indexes $j, k = 1, 2, 3$ and $j \neq k$.

Following Lemma 1, we have

$$\frac{1}{4}\boldsymbol{J}_i^{\top}(\boldsymbol{q})\boldsymbol{J}_i(\boldsymbol{q})\boldsymbol{q} = \boldsymbol{q}. \tag{28}$$

Then, the operator is simplified from a nonlinear multiplicative function with time complexity of $O(n^2)$ to a linear one with the complexity of $O(n)$

$$\boldsymbol{\Sigma}(\boldsymbol{q}) = \sum_{i\in\{w,v,\cdots,n\}} a_i \begin{bmatrix} \boldsymbol{I} - D^r_{x,i}\boldsymbol{M}_1(\boldsymbol{D}_i^b) \\ -D^r_{y,i}\boldsymbol{M}_2(\boldsymbol{D}_i^b) - D^r_{z,i}\boldsymbol{M}_3(\boldsymbol{D}_i^b) \end{bmatrix}. \tag{29}$$

The GDA measurement update equation finally arrives at

$$\boldsymbol{q}_{\boldsymbol{y},k} = \boldsymbol{q}_{\boldsymbol{y},k-1} - 2\chi_k \boldsymbol{\Sigma}(\boldsymbol{q}_{\boldsymbol{y},k-1})\boldsymbol{q}_{\boldsymbol{y},k-1} \tag{30}$$

where subscript $\boldsymbol{y}$ denotes the observation model source. This simplification converts the original $4 \times 3n$-by-$3n \times 1$ matrix multiplication $\boldsymbol{J}^{\top}_{\{w,v,\cdots,n\}}\boldsymbol{F}(\boldsymbol{q})$ to an additive sum of 4×4 matrices, which decreases the space complexity of the algorithm.

IV. Complementary Filter

A. Filter Design

A LCF can be written as the following observer [51]:

$$\begin{cases} \hat{\boldsymbol{x}}_k = \boldsymbol{\Phi}\hat{\boldsymbol{x}}_{k-1} + \boldsymbol{L}(\boldsymbol{y}_k - \hat{\boldsymbol{y}}_k) \\ \hat{\boldsymbol{y}}_k = \boldsymbol{H}\hat{\boldsymbol{x}}_k \end{cases} \tag{31}$$

where k denotes the kth time epoch, $\boldsymbol{x}$ denotes the state vector, and $\boldsymbol{y}$ denotes the measurement vector. $\boldsymbol{\Phi}$ and $\boldsymbol{H}$ are the transition matrix and measurement matrix, respectively. $\boldsymbol{L}$ is the feedback gain matrix. $\hat{\boldsymbol{p}}_k$ stands for the estimation of the $\boldsymbol{p}$ at epoch k. The feedback gain matrix $\boldsymbol{L}$ is empirically diagonal but may degenerates to a constant for convenience of implementation and gain determination when

$$\boldsymbol{L} = \beta \boldsymbol{I} \tag{32}$$

where β denotes a constant scalar [38]. If the state vector is the quaternion $\boldsymbol{q}$ in our case, the linear observer can be further designed as

$$\begin{cases} \hat{\boldsymbol{q}}_k = \boldsymbol{\Phi}\hat{\boldsymbol{q}}_{k-1} + \boldsymbol{L}(\boldsymbol{q}_{\boldsymbol{y},k} - \hat{\boldsymbol{q}}_{\boldsymbol{y},k}) \\ \hat{\boldsymbol{q}}_{\boldsymbol{y},k} = \boldsymbol{H}\hat{\boldsymbol{q}}_k \end{cases} \tag{33}$$

where

$$\boldsymbol{H} = \boldsymbol{I}. \tag{34}$$

Using the angular rate $\boldsymbol{\omega} = (\omega_x, \omega_y, \omega_z)^{\top}$, this equation generally leads to the following quaternion kinematic equation, such that [52]

$$\frac{d\boldsymbol{q}}{dt} = \frac{1}{2}[\boldsymbol{\Omega}\times]\boldsymbol{q} \tag{35}$$

where $[\boldsymbol{\Omega}\times]$ defines the skew symmetric matrix of angular rate in the Hamilton space $\boldsymbol{\Omega} = (0, \omega_x, \omega_y, \omega_z)^{\top}$

$$[\boldsymbol{\Omega}\times] = \begin{pmatrix} 0 & -\omega_x & -\omega_y & -\omega_z \\ \omega_x & 0 & \omega_z & -\omega_y \\ \omega_y & -\omega_z & 0 & \omega_x \\ \omega_z & \omega_y & -\omega_x & 0 \end{pmatrix}. \tag{36}$$

Hence, we approximately have [53]

$$\boldsymbol{\Phi} \approx \boldsymbol{I} + \frac{\Delta t}{2}[\boldsymbol{\Omega}\times] \tag{37}$$

where Δt denotes the time span. Expanding the state process equation, (33) can be further given by

$$\begin{aligned} \hat{\boldsymbol{q}}_k &= \boldsymbol{\Phi}\hat{\boldsymbol{q}}_{k-1} + \boldsymbol{L}(\boldsymbol{q}_{\boldsymbol{y},k} - \hat{\boldsymbol{q}}_{\boldsymbol{y},k}) \\ &\Rightarrow (\boldsymbol{I} + \boldsymbol{L})\hat{\boldsymbol{q}}_k = \boldsymbol{q}_{\omega,k} + \boldsymbol{L}\boldsymbol{q}_{\boldsymbol{y},k} \\ &\Rightarrow \hat{\boldsymbol{q}}_k = (\boldsymbol{I} + \boldsymbol{L})^{-1}(\boldsymbol{q}_{\omega,k} + \boldsymbol{L}\boldsymbol{q}_{\boldsymbol{y},k}) \\ &\Rightarrow \hat{\boldsymbol{q}}_k = (\boldsymbol{I} + \boldsymbol{L})^{-1}\boldsymbol{q}_{\omega,k} + (\boldsymbol{I} + \boldsymbol{L})^{-1}\boldsymbol{L}\boldsymbol{q}_{\boldsymbol{y},k} \\ &\Rightarrow \hat{\boldsymbol{q}}_k = (\boldsymbol{I} + \boldsymbol{L})^{-1}\boldsymbol{q}_{\omega,k} + (\boldsymbol{L}^{-1} + \boldsymbol{I})^{-1}\boldsymbol{q}_{\boldsymbol{y},k} \end{aligned} \tag{38}$$

where

$$\begin{cases} \boldsymbol{q}_{\boldsymbol{y},k} = [\boldsymbol{I} - 2\chi_k \boldsymbol{\Sigma}(\hat{\boldsymbol{q}}_{k-1})]\hat{\boldsymbol{q}}_{k-1} \\ \boldsymbol{q}_{\omega,k} = \left\{\boldsymbol{I} + \dfrac{\Delta t}{2}[\boldsymbol{\Omega}\times]\right\}\hat{\boldsymbol{q}}_{k-1}. \end{cases} \tag{39}$$

Let the complementary gain $\boldsymbol{G} = (\boldsymbol{L}^{-1} + \boldsymbol{I})^{-1}$, (38) can be given by

$$\begin{aligned} \hat{\boldsymbol{q}}_k &= (\boldsymbol{I} + \boldsymbol{L})^{-1}\boldsymbol{q}_{\omega,k} + (\boldsymbol{L}^{-1} + \boldsymbol{I})^{-1}\boldsymbol{q}_{\boldsymbol{y},k} \\ &= (\boldsymbol{I} - \boldsymbol{G})\boldsymbol{q}_{\omega,k} + \boldsymbol{G}\boldsymbol{q}_{\boldsymbol{y},k} \\ &= \left\{ \begin{array}{l} \boldsymbol{G}[\boldsymbol{I} - 2\chi_k \boldsymbol{\Sigma}(\hat{\boldsymbol{q}}_{k-1})] \\ \quad +(\boldsymbol{I} - \boldsymbol{G})\left(\boldsymbol{I} + \dfrac{\Delta t}{2}[\boldsymbol{\Omega}\times]\right) \end{array} \right\}\hat{\boldsymbol{q}}_{k-1} \\ &= \left\{\boldsymbol{I} + \frac{\Delta t}{2}(\boldsymbol{I} - \boldsymbol{G})[\boldsymbol{\Omega}\times] - 2\chi_k \boldsymbol{G}\boldsymbol{\Sigma}(\hat{\boldsymbol{q}}_{k-1})\right\}\hat{\boldsymbol{q}}_{k-1}. \end{aligned} \tag{40}$$

B. Robustness Ensurance

As described before, the measurement from vector observations compensates for the gyro bias. However, when highly dynamic conditions take place, the performance of the filter will be significantly affected. For instance, in previous works, when exposed to large external acceleration or magnetic distortion, the filter is influenced at the same time. In this paper, we invent a new way for norm verification to reject sensor outliers and, thus, make the proposed algorithm more robust.

The Euclidean norm information can be obtained during data acquisition of the ith sensor, such that

$$\text{Norm}_i = \|\boldsymbol{D}_i^b\| = \sqrt{\left(D_{x,i}^b\right)^2 + \left(D_{y,i}^b\right)^2 + \left(D_{z,i}^b\right)^2}. \tag{41}$$

Before the filtering process, we should have some priori knowledge of the adopted sensor. For any sensor, when it is operated with smooth motion under environments with stable external field, e.g., gravity field and earth-magnetic field, the norm of the output should be around a certain constant. We call this constant the standard norm $STDNorm_i$. When the motion becomes drastic, the norm of the sensor output will have relatively big deviation from the standard norm. In this circumstance, the sensor is no longer trustworthy and associated item in $\boldsymbol{\Sigma}(\hat{\boldsymbol{q}}_{k-1})$ should be deleted. Hence, the weights in (24) should be revised in this case as

$$\tilde{a}_i = \begin{cases} a_i, & |\text{Norm}_i - \text{STDNorm}_i| < \mu_i \\ 0, & |\text{Norm}_i - \text{STDNorm}_i| \geq \mu_i \end{cases} \tag{42}$$

and μ_i denotes a threshold for detecting drastic modes [15]. Finally, the whole filtering process including data acquisition and state update is given in Algorithm 1.

C. Determination of Parameters

There are some parameters to be determined before the filter begins. The initial quaternion $\boldsymbol{q}_{\text{init}}$ is the initial state of the attitude estimator and it can be obtained using initial alignment from strapdown sensors [28]. The complementary gain $\boldsymbol{G}$ is commonly set as a diagonal matrix whose components are empirically adjusted using the estimator's response. The determination of step length χ_0 is very similar. The weights can be determined using the initial standard deviations of different sensors [54]. When the robust ensurance step is applied, the standard norm list can be given according to the regular ranges of the sensors' norms. The thresholds are chosen empirically in terms of the smoothness of the filter, i.e., it decides how many "unusual" sensor observations with unusual norms are neglected.

Algorithm 1 GCF Using Strapdown Vector Observations via GDA (GCF)

Initialize:
Time epoch $k = 0$
Initial state $\boldsymbol{q}_{k=0} = \boldsymbol{q}_{init}$
Complementary gain $\boldsymbol{G}$
Step length $\chi_k = \chi_0$
Sorted valid sensors' indexes $w, v, \cdots, n$
Weights $a_w, a_v, \cdots, a_n$
Standard norm list $\{STDNorm_i | i = w, v, \cdots, n\}$
Threshold list $\{\mu_w, \mu_v, \cdots, \mu_n\}$
Output: $\hat{\boldsymbol{q}}_k$.
while no stop commands received **do**

1) $k = k + 1$
2) **Input:**
   a) Valid normalized strapdown sensor observations: $\boldsymbol{D}_w^b, \boldsymbol{D}_v^b, \cdots, \boldsymbol{D}_n^b$
   b) Normalized reference vectors: $\boldsymbol{D}_w^r, \boldsymbol{D}_v^r, \cdots, \boldsymbol{D}_n^r$
   c) Angular rate in (rad/s): $\boldsymbol{\omega} = \left(\omega_x, \omega_y, \omega_z\right)^\top$
   d) **If gyroscope is not valid:** $\boldsymbol{G} = \boldsymbol{I}$
3) Calculate norms $Norm_i = \left\|\boldsymbol{D}_i^b\right\|$
4) Deduce outlier rejection:
$$\tilde{a}_i = \begin{cases} a_i, |Norm_i - STDNorm_i| < \mu_i \\ 0, |Norm_i - STDNorm_i| \geq \mu_i \end{cases}$$
5) Normalization: $\boldsymbol{D}_i^b = \frac{\boldsymbol{D}_i^b}{\|\boldsymbol{D}_i^b\|}$
6) Calculate:
$$\widetilde{\boldsymbol{\Sigma}}(\hat{\boldsymbol{q}}_{k-1}) = \sum_{i\in\{w,v,\cdots,n\}} \tilde{a}_i \begin{bmatrix} \boldsymbol{I} - D_{x,i}^r \boldsymbol{M}_1(\boldsymbol{D}_i^b) \\ -D_{y,i}^r \boldsymbol{M}_2(\boldsymbol{D}_i^b) \\ -D_{z,i}^r \boldsymbol{M}_3(\boldsymbol{D}_i^b) \end{bmatrix}$$
7) Perform time update:
$$\hat{\boldsymbol{q}}_k = \left\{ \begin{array}{l} \boldsymbol{I} + \dfrac{\Delta t}{2}(\boldsymbol{I} - \boldsymbol{G})[\boldsymbol{\Omega}\times] \\ \quad -2\chi_k \boldsymbol{G}\widetilde{\boldsymbol{\Sigma}}(\hat{\boldsymbol{q}}_{k-1}) \end{array} \right\}\hat{\boldsymbol{q}}_{k-1}$$
8) Normalization: $\hat{\boldsymbol{q}}_k = \frac{\hat{\boldsymbol{q}}_k}{\|\hat{\boldsymbol{q}}_k\|}$

end while

D. Initial Alignment

The initial alignment problem is in fact the attitude determination from strapdown vector observations in the initial stage. The following scheme is depicted for initial alignment with our proposed filter:

$$\begin{aligned} \boldsymbol{q}_{\text{init},k} &= \boldsymbol{q}_{\text{init},k-1} - \boldsymbol{\Sigma}(\boldsymbol{q}_{\text{init},k-1})\boldsymbol{q}_{\text{init},k-1} \\ &\qquad \textbf{while } \|\boldsymbol{q}_{\text{init},k-1} - \boldsymbol{q}_{\text{init},k-2}\| > \kappa \end{aligned} \tag{43}$$

in which $k = 1, 2, \cdots$ and κ is the threshold indicating the relative accuracy. More specifically, in steady state, we have

$$\boldsymbol{\Sigma}(\boldsymbol{q}_{\text{init}})\boldsymbol{q}_{\text{init}} = \boldsymbol{0}. \tag{44}$$

Expanding it, the initial quaternion belongs to the following eigenvalue problem:

$$\begin{pmatrix} \sum\limits_{i\in\{w,v,\cdots,n\}} \begin{matrix} D^r_{x,i}\boldsymbol{M}_1(\boldsymbol{D}^b_i) \\ +D^r_{y,i}\boldsymbol{M}_2(\boldsymbol{D}^b_i) \\ +D^r_{z,i}\boldsymbol{M}_3(\boldsymbol{D}^b_i) \end{matrix} \end{pmatrix} \boldsymbol{q}_{\text{init}} = \boldsymbol{q}_{\text{init}}. \tag{45}$$

The optimal solution is the eigenvector associated with the eigenvalue closest to 1, which can be solved with our recent method FLAE [49].

E. Further Identities and Equivalences

Remark 1: Recalling (30), we can rewrite it as

$$\begin{aligned} \boldsymbol{q}_{\boldsymbol{y},k} &= \boldsymbol{q}_{\boldsymbol{y},k-1} - 2\chi_k \boldsymbol{\Sigma}(\boldsymbol{q}_{\boldsymbol{y},k-1})\boldsymbol{q}_{\boldsymbol{y},k-1} \\ &= \boldsymbol{q}_{\boldsymbol{y},k-1} - 2\chi_k \left\{ \boldsymbol{I} - \sum_{i\in\{w,v,\cdots,n\}} a_i \begin{bmatrix} D^r_{x,i}\boldsymbol{M}_1(\boldsymbol{D}^b_i) \\ +D^r_{y,i}\boldsymbol{M}_2(\boldsymbol{D}^b_i) \\ +D^r_{z,i}\boldsymbol{M}_3(\boldsymbol{D}^b_i) \end{bmatrix} \right\} \\ &\quad \times \boldsymbol{q}_{\boldsymbol{y},k-1} \\ &= (1-2\chi_k)\boldsymbol{q}_{\boldsymbol{y},k-1} + 2\chi_k \sum_{i\in\{w,v,\cdots,n\}} a_i \begin{bmatrix} D^r_{x,i}\boldsymbol{M}_1(\boldsymbol{D}^b_i) \\ +D^r_{y,i}\boldsymbol{M}_2(\boldsymbol{D}^b_i) \\ +D^r_{z,i}\boldsymbol{M}_3(\boldsymbol{D}^b_i) \end{bmatrix} \boldsymbol{q}. \end{aligned} \tag{46}$$

If we treat the step size as a complimentary gain, then observation model actually leads to a filtered quaternion. This shows that the GDA is not only an optimization solver but also a smoother as well. Such identity makes the obtained attitude estimates smoother than that directly derived from Wahba's solutions.

Theorem 2: Derivative-based optimization methods including GDA, GNA, and LMA for optimal attitude determination from vector observations are essentially equivalent to each other.

Proof: The GNA is a classical optimization problem, but it may fail when the Jacobian matrix is singular. Consequently, some other algorithms, e.g., the LMA, are designed to overcome this drawback. The searching equation can be written as

$$\begin{aligned} \boldsymbol{q}_k = \boldsymbol{q}_{k-1} - &\left(\boldsymbol{J}^\top_{\{w,v,\cdots n\}}\boldsymbol{J}_{\{w,v,\cdots n\}} + \lambda\boldsymbol{I}\right)^{-1} \\ &\times \boldsymbol{J}^\top_{\{w,v,\cdots n\}}\boldsymbol{f}(\boldsymbol{q}_{k-1}, \{w, v, \cdots n\}). \end{aligned} \tag{47}$$

Then, we have

$$\begin{aligned} &(\boldsymbol{J}^\top_{\{w,v,\cdots,n\}}\boldsymbol{J}_{\{w,v,\cdots,n\}} + \lambda\boldsymbol{I})\boldsymbol{q}_k \\ &\quad = (\boldsymbol{J}^\top_{\{w,v,\cdots,n\}}\boldsymbol{J}_{\{w,v,\cdots,n\}} + \lambda\boldsymbol{I})\boldsymbol{q}_{k-1} \\ &\qquad - \boldsymbol{J}^\top_{\{w,v,\cdots,n\}}\boldsymbol{f}(\boldsymbol{q}_{k-1}, \{w, v, \cdots, n\}). \end{aligned} \tag{48}$$

Note that

$$\begin{aligned} &(\boldsymbol{J}^\top_{\{w,v,\cdots,n\}}\boldsymbol{J}_{\{w,v,\cdots,n\}} + \lambda\boldsymbol{I})\boldsymbol{q}_{k-1} \\ &\quad = (\lambda\boldsymbol{I} + \sum_{i\in\{w,v,\cdots,n\}} a_i \boldsymbol{J}_i^\top \boldsymbol{J}_i)\boldsymbol{q}_{k-1} \\ &\quad = (1+\lambda)\boldsymbol{q}_{k-1}. \end{aligned} \tag{49}$$

Defining the quaternion error as

$$\Delta\boldsymbol{q} = \left(\boldsymbol{J}^\top_{\{w,v,\cdots,n\}}\boldsymbol{J}_{\{w,v,\cdots,n\}} + \lambda\boldsymbol{I})(\boldsymbol{q}_k - \boldsymbol{q}_{k-1}\right) \tag{50}$$

which is fully relevant to the original quaternion error $\boldsymbol{q}_k - \boldsymbol{q}_{k-1}$, according to invertible priori matrix multiplication, we finally obtain

$$\begin{aligned} \Delta\boldsymbol{q} \approx (1+\lambda)(\boldsymbol{q}_k - \boldsymbol{q}_{k-1}) \\ - \boldsymbol{J}^\top_{\{w,v,\cdots,n\}}\boldsymbol{f}(\boldsymbol{q}_{k-1}, \{w, v, \cdots, n\}). \end{aligned} \tag{51}$$

In other words, the LMA obtains the same optimization results in steady state with GDA. This shows that GDA is sufficient for optimization update and LMA-based method like [40] would only produce advance in smoothness. In addition, notice that LMA is, in fact, an improved algorithm based on GNA. This shows that related GNA methods like [38] are equivalent to the proposed GDA as well. As the mentioned GNA, LMA, and GDA are representatives of derivative-based optimization, the equivalence connections are established. ■

V. Hardware, Experiments, and Results

A. Sensors

Employed sensors in this section are a three-axis microelectromechanical system (MEMS) accelerometer, a three-axis MEMS gyroscope, a three-axis MEMS magnetometer, and a monocular camera. Each sensor has its sensing principle and mathematical model. Here, we simply introduce the details of these sensors.

A three-axis accelerometer measures the object's specific force. Its output in the object's body frame can be expressed by $\boldsymbol{A}^b = (a_x, a_y, a_z)^\top$. A three-axis gyroscope gives the angular rate data of the object and its output is given by $\omega = (\omega_x, \omega_y, \omega_z)^\top$. The magnetometer measures Earth's geomagnetic field and its output is $\boldsymbol{M}^b = (m_x, m_y, m_z)^\top$.

Camera has been widely used with the development of consumer electronics. Using a camera, we can capture numbers of images and videos. In fact, motion can be extracted from a recorded video stream since continuous pictures correspond to changes in attitude and translation. To achieve this task, the characteristics of pictures are necessary. There are many feature extraction methods including scale-invariant feature transform (SIFT) [55], gradient location-orientation histogram [56], speeded-up robust features [57], and so on. Extracted features from two neighboring images are in a degree similar. This provides an approach to determine the attitude and the translation vector with respect to the previous acquired image. Since the correlation of the 3-D features is easily disturbed by noises, the random sample consensus (RANSAC) algorithm [58] can be used for rejecting outliers according to probabilistic functions. Using the final valid features' correspondence, the relative attitude can be obtained from (3) via the SVD method by Arun *et al.* [44]. If the vision field is wide enough and the motion is relatively moderate, the attitude of the object can be directly obtained using the difference between the current and initial images.

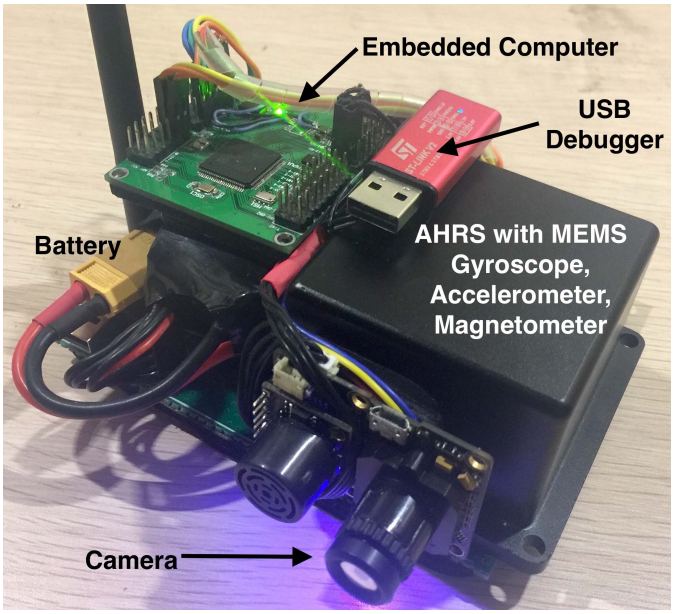

Fig. 1. Designed hardware platform. The platform consists of integrated AHRS, a monocular camera, a battery, a USB debugger, and an embedded computer.

B. Hardware Configuration

To verify the effectiveness of the proposed filter, an experimental platform is designed (see Fig. 1). The system integrates a commercial attitude and heading reference system (AHRS) which is composed of MARG sensors. The AHRS can give high-precision reference attitude angles along with raw sensor outputs and has been widely verified for its high reliability in navigation tasks such as UAV, land vehicles, and robots. The reference attitude angles from the AHRS are chosen as the ground truth. A camera is attached firmly to the installed AHRS to maintain relatively identical attitude determination. It should be noted that the design of the camera is motivated by PX4FLOW [59] but has been modified for broader vision field and higher image resolution. In fact, there is a microcontroller on the camera board making the calculations faster. The navigation computer is formed by an STM32F4-based board with multiple interfaces. To achieve wireless and highly reliable data transmission, an Xbee Pro S3B telemetry is installed on board.

In Sections V-C–V-F, we are going to carry out several experiments with the above-mentioned sensors in order to evaluate the performances of accuracy, robustness, and time consumption of the proposed algorithm compared with representative methods as follows.

1) The first one integrates a gyroscope, an accelerometer, and a magnetometer together which generates a typical full-attitude AHRS. In such combination, the vector pairs are

$$\begin{cases} \boldsymbol{D}_1^b = (a_x, a_y, a_z)^T \\ \boldsymbol{D}_2^b = (m_x, m_y, m_z)^T \end{cases} \quad \begin{cases} \boldsymbol{D}_1^r = (0, 0, 1)^T \\ \boldsymbol{D}_2^r = (m_N, 0, m_D)^T \end{cases} \tag{52}$$

where a_x, a_y, a_z and m_x, m_y, m_z are the normalized vector measurements in the body frame b from the accelerometer and magnetometer, respeceively. m_N and m_D are the reference vector components of the magnetometer in the North-East-Down frame which can be referenced from the geomagnetic model according to local geodetic location.

2) The second experiment involves a gyroscope, an accelerometer, a magnetometer, and a monocular camera in a hovering flight, where the vector pairs are

$$\begin{cases} \boldsymbol{D}_1^b = (a_x, a_y, a_z)^T \\ \boldsymbol{D}_2^b = (m_x, m_y, m_z)^T \\ \boldsymbol{D}_3^b = (p_{x,1}, p_{y,1}, p_{z,1})^T \\ \quad \vdots \\ \boldsymbol{D}_n^b = \begin{pmatrix} p_{x,n-2}, \\ p_{y,n-2}, p_{z,n-2} \end{pmatrix}^T \end{cases}, \quad \begin{cases} \boldsymbol{D}_1^r = (0, 0, 1)^T \\ \boldsymbol{D}_2^r = (m_N, 0, m_D)^T \\ \boldsymbol{D}_3^r = (p_{x,1}^r, p_{y,1}^r, p_{z,1}^r)^T \\ \quad \vdots \\ \boldsymbol{D}_n^r = \begin{pmatrix} p_{x,n-2}^r, \\ p_{y,n-2}^r, p_{z,n-2}^r \end{pmatrix}^T \end{cases} \tag{53}$$

in which $p_{x,i}, p_{y,i}, p_{z,i}$ are the normalized coordinates of the ith transformed feature points in the body frame. $p_{x,i}^r, p_{y,i}^r, p_{z,i}^r$ are the normalized ith transformed feature points reference obtained in initial image capture of the ground.

With vector pair configurations shown earlier, we can easily fuse them with the procedure provided in Algorithm 1.

C. Case 1: AHRS With MARG Sensors

The accelerometer and magnetometer are introduced, adding a compensation of pitch, roll, and yaw angles from gravity-field and magnetic-field sensing data. The MARG sensors are calibrated for initial biases and misalignment. To ensure good results, the operating temperature of the sensors is stablized at 45°C using a controlled thermal resistance. Constant iron and soft magnetic distortion to the magnetometer are also compensated for before all the experiments [60]. To verify the performance of the proposed generalized CF (GCF), representative methods such as Wahba's CF (WCF) by Marantos *et al.* [19], Algebraic-QUaternion-Algorithm-based quaternion KF (AQUA q-KF) by Valenti *et al.* [23], and LMA complementary observer (LMA-CO) by Fourati *et al.* [40] are used for comparisons. The parameters of different filters are tuned as follows.

1) WCF: The parameters are $w_a = 0.9, w_m = 0.8, c_1^a = c_1^m = 0.7, c_2^a = c_2^m = 0.3, c_3^a = 8500, c_3^m = 5500$ as described in [19].
2) AQUA q-KF: The variance matrices are

$$\begin{aligned} \boldsymbol{\Sigma}_{\text{gyro}} &= \text{diag}(0.0013, 0.0013, 0.0013) \\ \boldsymbol{\Sigma}_{\text{acc}} &= \text{diag}(0.01, 0.01, 0.02) \\ \boldsymbol{\Sigma}_{\text{mag}} &= \text{diag}(0.05, 0.05, 0.05). \end{aligned}$$

3) LMA-CO: The gain is set to 0.1 and the positive number for LMA is set to $\lambda = 0.000001$.
4) Proposed GCF: The weights are set to $a_{\text{acc}} = 0.7$ and $a_{\text{mag}} = 0.3$ to enhance the accelerometer's effect while the complementary gain is set to $\boldsymbol{G} = 0.1\boldsymbol{I}$. The gain of the proposed GCF is tuned to achieve relatively good attitude estimation results in the case of such experimental conditions.

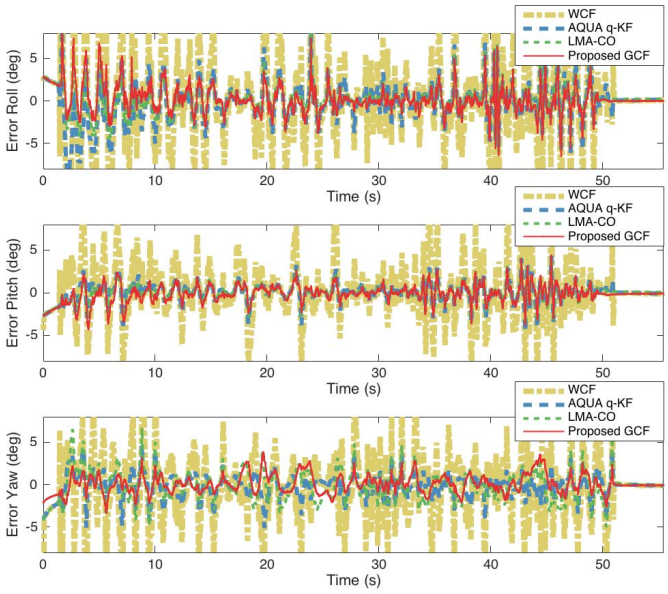

Fig. 2. Attitude estimation errors during a flat motion from WCF, AQUA q-KF, LMA-CO, and the proposed GCF. Accelerometer and magnetometer are jointly utilized.

TABLE I
RMSEs OF ATTITUDE ANGLES

Algorithms	Roll	Pitch	Yaw
WCF	4.5075°	2.7846°	3.5715°
AQUA q-KF	2.1736°	1.0264°	1.3266°
LMA-CO	1.6172°	1.0539°	1.7120°
Proposed GCF	1.6018°	1.0107°	1.0998°

With the recorded data in the previous experiment, the attitude estimation errors are obtained and shown in Fig. 2. In this evaluation, the norm verification is not performed since the motion is not drastic. As can be seen from the figure, WCF is the worst among all filters. The estimation accuracy of AQUA q-KF and LMA-CO is close to that of the proposed filter. To further verify the performances, we calculate the root-mean-squared errors (RMSEs) of various algorithms with respect to reference angles from high precision AHRS (see Table I).

We can see that for roll and pitch angles, the proposed GCF reaches almost the same accuracy with LMA-CO while GCF is the best for estimating attitude angles. This shows that the proposed GCF is efficient for quasi-static attitude estimation.

As described before, the performance of the filter is being tested out when drastic conditions occur. The magnetometer can be easily disturbed by iron or magnetic objects, i.e., it is sensitive to magnetic distortion. In the next experiment, the designed hardware remains still on a table and is perturbed by a moving magnet. Fig. 3 reflects the raw data from the magnetometer along with its norm. We can see that the magnetic distortion is very large with the norm of up to 10 Gauss. Using the acquired data, attitude estimation errors are calculated and shown in Fig. 4. The threshold for norm verification of magnetometer is set to $\mu_{\text{mag}} = 0.2$. We can

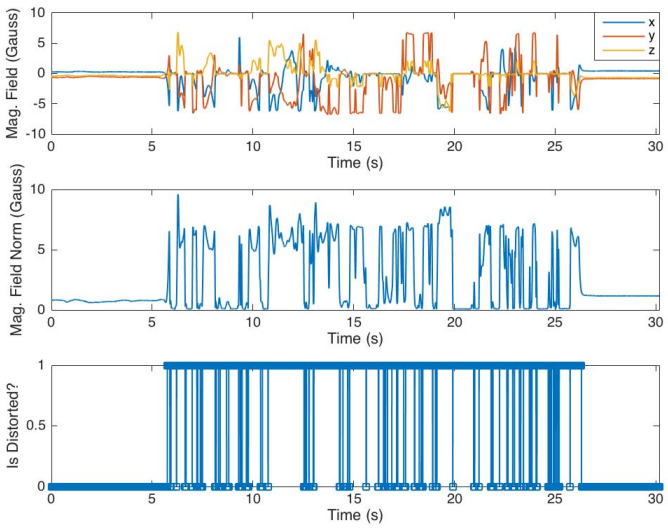

Fig. 3. (a) Raw data from magnetometer. (b) Norm of the measured magnetic field. (c) Modes of the motion.

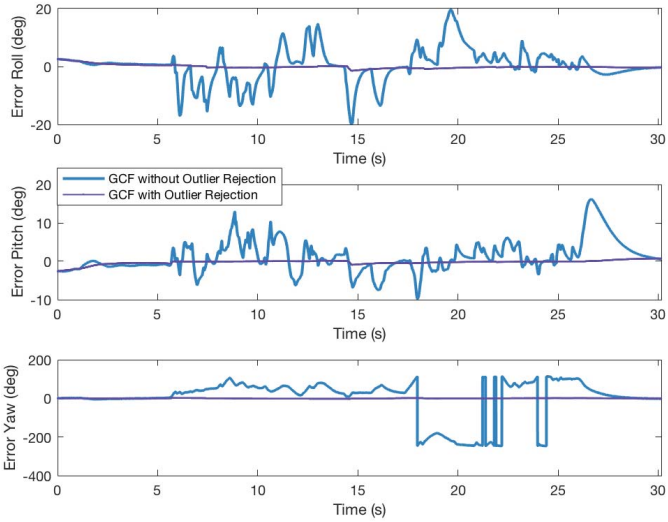

Fig. 4. Attitude errors from various sources in the presence of magnetic distortion.

find out that the filter without outlier rejection undergoes very evident disturbances of yaw angles as magnetic distortion happens. The proposed GCF is disturbed, in this case, not only for yaw but also for roll and pitch angles. However, GCF with outlier rejection shows interesting behavior since it is hardly perturbed by the magnetic distortion. The third figure of Fig. 3 shows that the filter can detect the magnetic distortion at a high level. Although most magnetometer's outputs are being disturbed, there are still some trustworthy data. Using these data, the filter maintains stable with convergent yaw estimation. The RMSEs are shown in Table II.

D. Case 2: MARG Sensors and a Monocular Camera

In this section, a quadrotor is used to carry the designed platform (see Fig. 5). The quadrotor is equipped with carbon-fiber body and propellers and is operated under human's control

TABLE II
RMSEs OF ATTITUDE ANGLES WHEN MAGNETIC DISTORTION TAKES PLACE

Algorithms	Roll	Pitch	Yaw
GCF with outlier rejection	0.6637°	0.5525°	1.1507°
GCF without outlier rejection	5.7659°	4.0821°	99.4968°

Fig. 5. Quadrotor is used for validation of the attitude estimation system involving MARG sensors and a monocular camera.

TABLE III
RMSEs OF ATTITUDE ANGLES

Algorithms	Roll	Pitch	Yaw
SVD	2.1848°	2.0441°	2.4495°
QUEST	1.4628°	1.0825°	1.9269°
Sergio's Observer	0.6998°	0.3990°	0.6816°
Proposed GCF	0.3798°	0.3377°	0.1731°

via a flight controller of DJI Wookong-M. The camera is precalibrated for its intrinsic parameters using the geometric method proposed by Zhang [61]. The 2-D feature points are converted to the 3-D camera frame via intrinsic parameters and instant rotation prediction from angular rate measurements. During a hovering flight, when the attitude and altitude are relatively stable, raw inertial data, raw images, and reference attitude angles are recorded with the frequency of 50 Hz. A certain image is chosen as the reference image. The images are processed with SIFT and RANSAC for point cloud matching. An amount of at least four point pairs and 12 point pairs at most are designed for the selecting of vector observations. All the point pairs are ensured not to be collinear with each other. The accelerometer and magnetometer are also adopted for sensor fusion.

The attitude estimation results are calculated with the proposed CF, an attitude observer proposed by Bras *et al.* [62], the SVD method proposed by Arun *et al.* [44], and the QUEST solution to Wahba's problem [47]. The related attitude angles are depicted in Fig. 6. As can be seen from the figure, the proposed filter's attitude estimation is the closest to reference angles. While for other algorithms, the variance is evidently larger than the proposed GCF. The RMSEs of the attitude angles from different sources are given in Table III. As the matter of fact, the proposed GDA method provides us with a new approach for attitude determination from

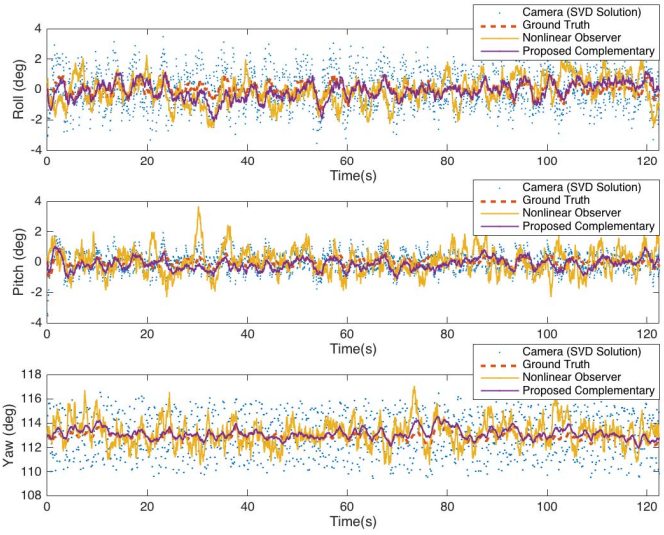

Fig. 6. Attitude estimation results from different sources. The "SVD solution" refers to Arun *et al.*'s [44] method while "nonlinear observer" is the algorithm developed by Bras *et al.* [62].

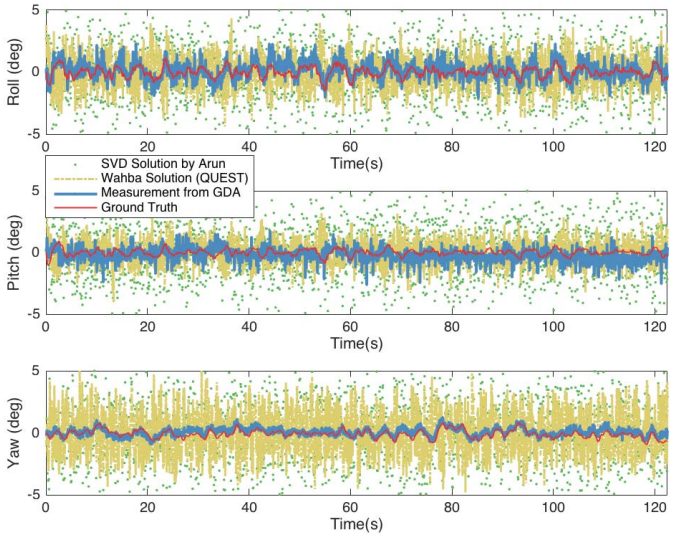

Fig. 7. Attitude estimation results from vector observations. The SVD solution proposed by Arun *et al.* [44], QUEST algorithm proposed by Shuster *et al.* [47], and the proposed GDA are adopted for comparisons.

vector observations. Using the raw data collected, the comparisons on attitude angles with various algorithms are depicted in Fig. 7. The results show that the batch attitude determination from SVD and Wahba's solution are much more noisy with respect to the proposed GDA. This indicates that the proposed GDA can properly determinate the attitude with smooth outputs. This can be applied to related areas for reliable attitude determination from camera outputs.

E. Evaluation of Open Data Sets

In today's autonomous driving equipments, there are always sensors such inertial measurement unit (IMU) and global navigation satellite system (GNSS) receiver to perform accurate state estimation of vehicles. The KITTI data set [63],

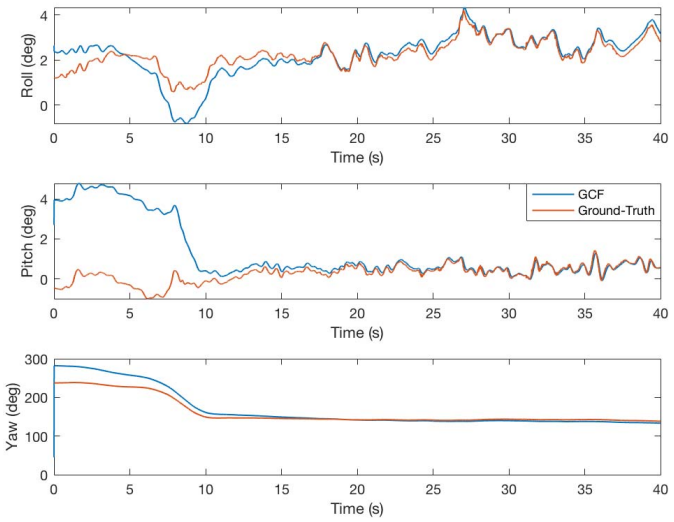

Fig. 8. Attitude estimation results using KITTI data set.

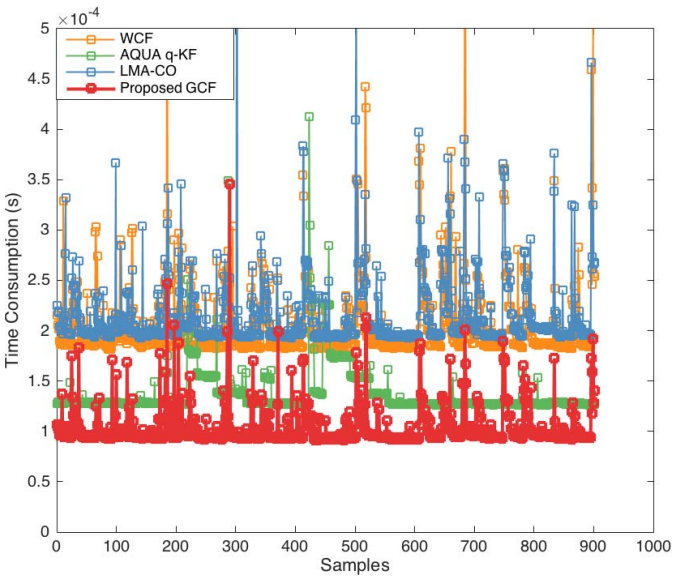

Fig. 9. Time consumption of different algorithms for MARG fusion.

released by the Karlsruhe Institute of Technology and Toyota Technological Institute at Chicago in 2012, has been widely employed in algorithmic evaluations in representative works. It provides the users with a large variety of sensor measurements including angular rate, acceleration, velocity, position, and ground-truth values. Here, we use the data set `2011_09_26_drive_0096_extract` in the city scenes. We use the accelerometer and GNSS velocity measurements to form the vector observation pairs such that

$$\begin{cases} \boldsymbol{D}_1^b = (a_{\mathcal{F}}, a_{\mathcal{L}}, a_{\mathcal{U}})^\top \\ \boldsymbol{D}_2^b = (0, -1, 0)^\top, \end{cases} \quad \begin{cases} \boldsymbol{D}_1^r = (0, 0, -1)^\top \\ \boldsymbol{D}_2^r = (v_{\mathcal{F}}, v_{\mathcal{L}}, v_{\mathcal{U}})^\top \end{cases}$$

where $a_{\mathcal{F}}, a_{\mathcal{L}}, a_{\mathcal{U}}$ and $v_{\mathcal{F}}, v_{\mathcal{L}}, v_{\mathcal{U}}$ are the normalized measurements of the acceleration and velocity, respectively, in the Forward-Top-Left frame. The weights of the two strapdown measurements are given equally, i.e., 0.5 and 0.5 [64]. The complementary gain is set to $\boldsymbol{G} = 0.01\boldsymbol{I}$ while the GDA step size is $\chi = 0.1$. The acceletometer-GNSS fusion is enabled only when the velocity norm is over 1m/s to ensure reliable and satisfactory heading determination. Filtering with the angular rate, the attitude results are computed in Fig. 8. The proposed GCF gradually converges to the ground truth over the initial time period. In fact, the filter's convergence largely depends on the filter gain and GDA correction step length. Here, the experimental result has proven the correctness and efficiency of the proposed filter. In later works, we will try to find how to adaptively tune the filter gain so that the attitude estimation would be closer to the ground truth all the time.

F. Time Consumption

This section shows the execution cost regarding the time consumption of the proposed filter. Several comparisons are conducted to verify the performances.

1) Comparisons With Various Algorithms: Most of the adopted algorithms in Sections V-C–V-E are evaluated for time consumption results. Fig. 9 shows the comparisons of time consumption between attitude algorithms for MARG fusion.

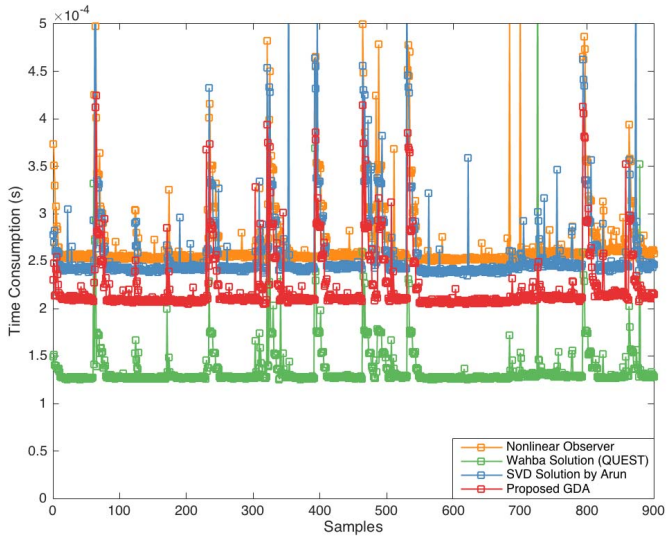

Fig. 10. Time consumption of different algorithms for attitude determination from camera outputs.

Among all the algorithms, the proposed GCF owns the least time consumption while LMA-CO is the slowest. The WCF, in fact, uses an SVD solution to Wahba's problem [45] to form a CF. LMA-CO requires the calculation of the Jacobian and inversion thus makes it slow. AQUA q-KF is based on KF theory which needs many matrix operations. The proposed filter, however, is free of inversion and other operations. Hence, in a word, the mathematical design of the proposed GCF makes it faster than other algorithms. When we use camera to obtain attitude determination, the amount of vector observations significantly increases. At this time, various algorithms have quite different behaviors. The related evaluated time consumption is given in Fig. 10.

We can see that the QUEST algorithm is the fastest among all algorithms. However, QUEST, as a batch attitude

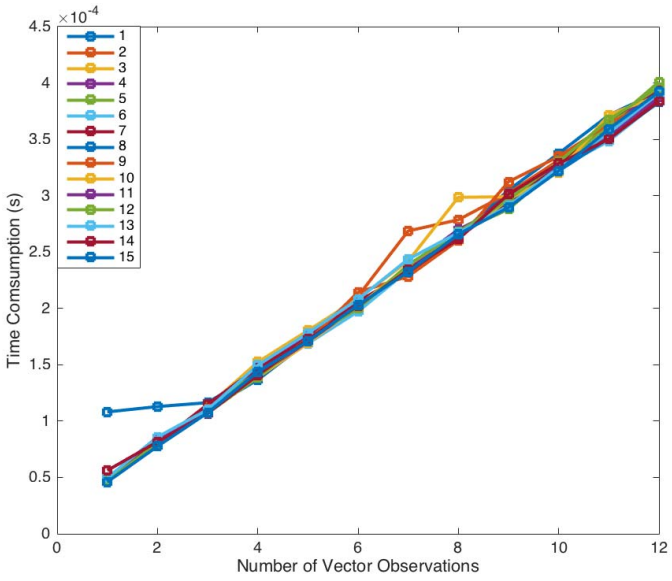

Fig. 11. Time consumption of the proposed filter varies with the amount of the vector observations. The legend denotes the index of the repeated simulation.

TABLE IV
MEAN AND STANDARD DEVIATION OF TIME CONSUMPTION OF VARIOUS ALGORITHMS FOR EACH VECTOR OBSERVATION. EACH ALGORITHM IS EXECUTED FOR 20× TO OBTAIN THE AVERAGE VALUES

Algorithms	Mean Time	STD
Proposed GCF	3.4141×10^{-5}s	2.9987×10^{-6}s
WCF	9.2680×10^{-5}s	9.1729×10^{-6}s
LMA-CO	9.9289×10^{-5}s	1.2806×10^{-5}s
AQUA q-KF	6.8710×10^{-5}s	1.1821×10^{-5}s
Nonlinear Observer	6.3368×10^{-5}s	8.2699×10^{-6}s
QUEST	2.9176×10^{-5}s	3.6136×10^{-6}s
SVD	5.4259×10^{-5}s	5.8520×10^{-6}s

determination algorithm, can only produce unfiltered results from vector observations. In real applications, we need smooth state estimates to ensure the operating quality of the system. It should be noted that the proposed GDA, as described before, can be seen as an attitude smoother (see Fig. 7). The results show that the proposed GDA is the second fastest among all the algorithms. This proves that the proposed GDA can determinate attitude with relatively fast speed and much more smooth outputs. The mean time consumption and related standard deviation of different algorithms are presented in Table IV.

2) Time Complexity Test: Numbers of simulations are also carried out to show the relationship between the amount of vector observations and time consumption. We repeated one simulation with various amount of vector observations for 15 times and the details are gathered and shown in Fig. 11. Multiple simulations show that the relationship is linear between the amount of vector observations and time consumption. Hence, this algorithm owns a time complexity of $O(n)$. The reason is that the proposed filter simplifies the computation of the Jacobian matrix and, thus, converts the sophisticated matrix multiplication to a sum of matrices. The low time complexity of the proposed filter makes it easy to be applied on platforms with low configurations. The saved time can be reserved for fault detection, failsafe, reliability enhancement, and so on.

VI. CONCLUSION

This paper deals with the generalized multisensor fusion problem. Based on some previous works, the problem is transformed into minimizing a new error function. The minimization problem is then solved using the GDA. Different from existing works, we obtain some meaningful findings of the sensor fusion that significantly simplifies the computation of the Jacobian matrix. The original huge matrix multiplication is then converted to a sum of several matrices. The proposed approach, in fact, gives a new perspective for attitude determination from vector observations. A CF is designed further to fuse the angular rate and measurement quaternion from vector observations together. The filter is then named as the GCF. Moreover, we study some mathematical properties of the proposed GCF. Results show that for quaternion-based attitude estimation from angular rate information and strapdown vector observations, the proposed GDA is equivalent to LMA.

Experiments and simulations are designed and carried out to verify the correctness and effectiveness of the proposed filter. Throughout the experiments using MARG sensors, the results prove that the proposed filter can produce accurate attitude estimation in both normal and harsh cases. The algorithm is then extended to attitude estimation using inertial information and visual data from a monocular camera. The comparisons show that the filter can also achieve a satisfactory attitude accuracy with respect to ground truth and other representative methods. Execution time consumption from various sources is also investigated which proves that the proposed filter is computation efficient and owns a time complexity of $O(n)$ with respect to the number of vector observations that makes it easier to be implemented on low-configuration platforms.

We believe that the proposed filter can potentially benefit related navigational applications. Related codes have been upload on https://github.com/zarathustr/GCF. Also, we think that the determination of an adaptive gain to the filter for better dynamic performance will be another task for us in the future.

APPENDIX
MANDATORY PROOFS

A. Linear Matrix Algebra

$$\boldsymbol{P}_1^{\top}(\boldsymbol{q})\boldsymbol{D}_i^b = \begin{pmatrix} D_{x,i}^b q_0 - D_{y,i}^b q_3 + D_{z,i}^b q_2 \\ D_{x,i}^b q_1 + D_{y,i}^b q_2 + D_{z,i}^b q_3 \\ D_{y,i}^b q_1 - D_{x,i}^b q_2 + D_{z,i}^b q_0 \\ D_{z,i}^b q_1 - D_{y,i}^b q_0 - D_{x,i}^b q_3 \end{pmatrix}$$

$$= \begin{pmatrix} D_{x,i}^b & 0 & D_{z,i}^b & -D_{y,i}^b \\ 0 & D_{x,i}^b & D_{y,i}^b & D_{z,i}^b \\ D_{z,i}^b & D_{y,i}^b & -D_{x,i}^b & 0 \\ -D_{y,i}^b & D_{z,i}^b & 0 & -D_{x,i}^b \end{pmatrix} \boldsymbol{q} = \boldsymbol{M}_1(\boldsymbol{D}_i^b)\boldsymbol{q}$$

$$\boldsymbol{P}_2^\top(\boldsymbol{q})\boldsymbol{D}_i^b = \begin{pmatrix} D_{x,i}^b q_3 + D_{y,i}^b q_0 - D_{z,i}^b q_1 \\ D_{x,i}^b q_2 - D_{y,i}^b q_1 - D_{z,i}^b q_0 \\ D_{x,i}^b q_1 + D_{y,i}^b q_2 + D_{z,i}^b q_3 \\ D_{x,i}^b q_0 - D_{y,i}^b q_3 + D_{z,i}^b q_2 \end{pmatrix} = \begin{pmatrix} D_{y,i}^b & -D_{z,i}^b & 0 & D_{x,i}^b \\ -D_{z,i}^b & -D_{y,i}^b & D_{x,i}^b & 0 \\ 0 & D_{x,i}^b & D_{y,i}^b & D_{z,i}^b \\ D_{x,i}^b & 0 & D_{z,i}^b & -D_{y,i}^b \end{pmatrix} \boldsymbol{q} = \boldsymbol{M}_2(\boldsymbol{D}_i^b)\boldsymbol{q}$$

$$\boldsymbol{P}_3^\top(\boldsymbol{q})\boldsymbol{D}_i^b = \begin{pmatrix} D_{y,i}^b q_1 - D_{x,i}^b q_2 + D_{z,i}^b q_0 \\ D_{x,i}^b q_3 + D_{y,i}^b q_0 - D_{z,i}^b q_1 \\ D_{y,i}^b q_3 - D_{x,i}^b q_0 - D_{z,i}^b q_2 \\ D_{x,i}^b q_1 + D_{y,i}^b q_2 + D_{z,i}^b q_3 \end{pmatrix} = \begin{pmatrix} D_{z,i}^b & D_{y,i}^b & -D_{x,i}^b & 0 \\ D_{y,i}^b & -D_{z,i}^b & 0 & D_{x,i}^b \\ -D_{x,i}^b & 0 & -D_{z,i}^b & D_{y,i}^b \\ 0 & D_{x,i}^b & D_{y,i}^b & D_{z,i}^b \end{pmatrix} \boldsymbol{q} = \boldsymbol{M}_3(\boldsymbol{D}_i^b)\boldsymbol{q}. \tag{54}$$

B. Quaternion Identities

One can easily write out

$$\boldsymbol{P}_1^\top(\boldsymbol{q})\boldsymbol{P}_1(\boldsymbol{q}) = \begin{pmatrix} q_0^2+q_2^2+q_3^2 & q_1q_0 & -q_1q_3 & q_1q_2 \\ q_0q_1 & q_1^2+q_2^2+q_3^2 & q_0q_3 & -q_0q_2 \\ -q_3q_1 & q_3q_0 & q_0^2+q_1^2+q_2^2 & q_2q_3 \\ q_1q_2 & -q_0q_2 & q_2q_3 & q_0^2+q_1^2+q_3^2 \end{pmatrix}. \tag{55}$$

With the same technique, we obtain

$$\begin{cases} \boldsymbol{P}_1^\top(\boldsymbol{q})\boldsymbol{P}_1(\boldsymbol{q}) = \boldsymbol{I}_{4\times4} + \boldsymbol{U}_1(\boldsymbol{q}) \\ \boldsymbol{P}_2^\top(\boldsymbol{q})\boldsymbol{P}_2(\boldsymbol{q}) = \boldsymbol{I}_{4\times4} + \boldsymbol{U}_2(\boldsymbol{q}) \\ \boldsymbol{P}_3^\top(\boldsymbol{q})\boldsymbol{P}_3(\boldsymbol{q}) = \boldsymbol{I}_{4\times4} + \boldsymbol{U}_3(\boldsymbol{q}) \end{cases} \tag{56}$$

where

$$\boldsymbol{U}_1(\boldsymbol{q}) = \begin{pmatrix} -q_1^2 & q_0q_1 & -q_1q_3 & q_1q_2 \\ q_0q_1 & -q_0^2 & q_0q_3 & -q_0q_2 \\ -q_1q_3 & q_0q_3 & -q_3^2 & q_2q_3 \\ q_1q_2 & -q_0q_2 & q_2q_3 & -q_2^2 \end{pmatrix} \tag{57a}$$

$$\boldsymbol{U}_2(\boldsymbol{q}) = \begin{pmatrix} -q_2^2 & q_2q_3 & q_0q_2 & -q_1q_2 \\ q_2q_3 & -q_3^2 & -q_0q_3 & q_1q_3 \\ q_0q_2 & -q_0q_3 & -q_0^2 & q_0q_1 \\ -q_1q_2 & q_1q_3 & q_0q_1 & -q_1^2 \end{pmatrix}$$

$$\boldsymbol{U}_3(\boldsymbol{q}) = \begin{pmatrix} -q_3^2 & -q_2q_3 & q_1q_3 & q_0q_3 \\ -q_2q_3 & -q_2^2 & q_1q_2 & q_0q_2 \\ q_1q_3 & q_1q_2 & -q_1^2 & -q_0q_1 \\ q_0q_3 & q_0q_2 & -q_0q_1 & -q_0^2 \end{pmatrix}. \tag{57b}$$

Then, with expansions, we have

$$\boldsymbol{U}_1(\boldsymbol{q})\boldsymbol{q} = \boldsymbol{U}_2(\boldsymbol{q})\boldsymbol{q} = \boldsymbol{U}_3(\boldsymbol{q})\boldsymbol{q} = \boldsymbol{0}_{4\times1} \tag{58}$$

which finishes the proof of Theorem 1.

ACKNOWLEDGMENT

The authors would like to thank Chengdu Bobei Inc. (AMOV Lab) and Beijing Sanchi Inertial Inc. for the related sensor services. They would like to thank Dr. F. L. Markley from NASA Goddard Space Flight Center and Prof. Y. Wu from Shanghai Jiao Tong University for their constructive comments, suggestions, and support. This paper is presented in memorial of Z. K. Wu, the grandfather of author J. Wu, who passed away during the composition of this paper.

REFERENCES

[1] M. Chan, D. Estève, J.-Y. Fourniols, C. Escriba, and E. Campo, "Smart wearable systems: Current status and future challenges," *Artif. Intell. Med.*, vol. 56, no. 3, pp. 137–156, Nov. 2012.

[2] H. Fourati, "Heterogeneous data fusion algorithm for pedestrian navigation via foot-mounted inertial measurement unit and complementary filter," *IEEE Trans. Instrum. Meas.*, vol. 64, no. 1, pp. 221–229, Jan. 2015.

[3] G. To and M. R. Mahfouz, "Quaternionic attitude estimation for robotic and human motion tracking using sequential Monte Carlo methods with von Mises–Fisher and nonuniform densities simulations," *IEEE Trans. Biomed. Eng.*, vol. 60, no. 11, pp. 3046–3059, Nov. 2013.

[4] J. Goslinski, M. Nowicki, and P. Skrzypczynski, "Performance comparison of EKF-based algorithms for orientation estimation on Android platform," *IEEE Sensors J.*, vol. 15, no. 7, pp. 3781–3792, Jul. 2015.

[5] T. Michel, H. Fourati, P. Genevès, and N. Layaïda, "A comparative analysis of attitude estimation for pedestrian navigation with smartphones," in *Proc. Int. Conf. Indoor Positioning Indoor Navigat. (IPIN)*, Oct. 2015, pp. 13–16.

[6] Y. Yuan, Z. Wang, and L. Guo, "Event-triggered strategy design for discrete-time nonlinear quadratic games with disturbance compensations: The noncooperative case," *IEEE Trans. Syst., Man, Cybern., Syst.*, vol. 48, no. 11, pp. 1885–1896, Nov. 2018.

[7] Y. Wu, D. Zou, P. Liu, and W. Yu, "Dynamic magnetometer calibration and alignment to inertial sensors by Kalman filtering," *IEEE Trans. Control Syst. Technol.*, vol. 26, no. 2, pp. 716–723, Mar. 2018.

[8] Z. Zhou, "Optimal batch distributed asynchronous multi-sensor fusion with feedback," *IEEE Trans. Aerosp. Electron. Syst.*, to be published, doi: 10.1109/TAES.2018.2847979.

[9] H. Liu, F. Sun, B. Fang, and X. Zhang, "Robotic room-level localization using multiple sets of sonar measurements," *IEEE Trans. Instrum. Meas.*, vol. 66, no. 1, pp. 2–13, Jan. 2017.

[10] F. Königseder, W. Kemmetmüller, and A. Kugi, "Attitude estimation using redundant inertial measurement units for the control of a camera stabilization platform," *IEEE Trans. Control Syst. Technol.*, vol. 24, no. 5, pp. 1837–1844, Sep. 2016.

[11] Y. Lee, Y. Kim, G. Moon, and B.-E. Jun, "Sliding-mode-based missile-integrated attitude control schemes considering velocity change," *J. Guid., Control, Dyn.*, vol. 39, no. 3, pp. 423–436, 2016.

[12] R. Li, Y. Song, and Y. Shi, "Multi-group coordination control of multi-agent system based on smoothing estimator," *IET Control Theory Appl.*, vol. 10, no. 11, pp. 1224–1230, 2016.

[13] Z. Zhou, Y. Li, J. Zhang, and C. Rizos, "Integrated navigation system for a low-cost quadrotor aerial vehicle in the presence of rotor influences," *J. Surveying Eng.*, vol. 143, no. 1, p. 05016006, 2017.

[14] A. Makni, H. Fourati, and A. Y. Kibangou, "Energy-aware adaptive attitude estimation under external acceleration for pedestrian navigation," *IEEE/ASME Trans. Mechatronics*, vol. 21, no. 3, pp. 1366–1375, Jun. 2016.

[15] W. Li and J. Wang, "Effective adaptive Kalman filter for MEMS-IMU/magnetometers integrated attitude and heading reference systems," *J. Navigat.*, vol. 66, no. 1, pp. 99–113, 2013.

[16] Z. Wu, Z. Sun, W. Zhang, and Q. Chen, "A novel approach for attitude estimation based on MEMS inertial sensors using nonlinear complementary filters," *IEEE Sensors J.*, vol. 16, no. 10, pp. 3856–3864, May 2014.

[17] Y. Wu, J. Wang, and D. Hu, "A new technique for INS/GNSS attitude and parameter estimation using online optimization," *IEEE Trans. Signal Process.*, vol. 62, no. 10, pp. 2642–2655, May 2014.

[18] L. Meier, P. Tanskanen, L. Heng, G. H. Lee, F. Fraundorfer, and M. Pollefeys, "PIXHAWK: A system for autonomous flight using onboard computer vision," *Auto. Robots*, vol. 33, nos. 1–2, pp. 21–39, 2012.

[19] P. Marantos, Y. Koveos, and K. J. Kyriakopoulos, "UAV state estimation using adaptive complementary filters," *IEEE Trans. Control Syst. Technol.*, vol. 24, no. 4, pp. 1214–1226, Jul. 2016.

[20] Z. Zhou, Y. Li, J. Liu, and G. Li, "Equality constrained robust measurement fusion for adaptive Kalman-filter-based heterogeneous multisensor navigation," *IEEE Trans. Aerosp. Electron. Syst.*, vol. 49, no. 4, pp. 2146–2157, Oct. 2013.

[21] R. E. Kalman, "A new approach to linear filtering and prediction problems," *Trans. ASME, D, J. Basic Eng.*, vol. 82, pp. 35–45, 1960.

[22] Y. Yuan, Z. Wang, and L. Guo, "Distributed quantized multi-modal H_∞ fusion filtering for two-time-scale systems," *Inf. Sci.*, vol. 432, pp. 572–583, Mar. 2018.

[23] R. G. Valenti, I. Dryanovski, and J. Xiao, "A linear Kalman filter for MARG orientation estimation using the algebraic quaternion algorithm," *IEEE Trans. Instrum. Meas.*, vol. 65, no. 2, pp. 467–481, Feb. 2016.

[24] A. M. Sabatini, "Quaternion-based extended Kalman filter for determining orientation by inertial and magnetic sensing," *IEEE Trans. Biomed. Eng.*, vol. 53, no. 7, pp. 1346–1356, Jul. 2006.

[25] J. L. Crassidis and F. L. Markley, "Unscented filtering for spacecraft attitude estimation," *J. Guid., Control, Dyn.*, vol. 26, no. 4, pp. 536–542, Jul. 2003.

[26] J. D. Gibson, B. Koo, and S. D. Gray, "Filtering of colored noise for speech enhancement and coding," *IEEE Trans. Signal Process.*, vol. 39, no. 8, pp. 1732–1742, Aug. 1991.

[27] F. L. Markley, "Attitude error representations for Kalman filtering," *J. Guid., Control, Dyn.*, vol. 26, no. 2, pp. 311–317, 2003.

[28] Y. S. Suh, "Orientation estimation using a quaternion-based indirect Kalman filter with adaptive estimation of external acceleration," *IEEE Trans. Instrum. Meas.*, vol. 59, no. 12, pp. 3296–3305, Dec. 2010.

[29] R. Kottath, P. Narkhede, V. Kumar, V. Karar, and S. Poddar, "Multiple model adaptive complementary filter for attitude estimation," *Aerosp. Sci. Technol.*, vol. 69, pp. 574–581, Oct. 2017.

[30] R. Kottath, P. Narkhede, V. Kumar, and A. Kumar, "PSO aided adaptive complementary filter for attitude estimation," *J. Intell. Robotic Syst.*, vol. 87, pp. 531–543, Sep. 2017.

[31] T. A. Johansen, J. M. Hansen, and T. I. Fossen, "Nonlinear observer for tightly integrated inertial navigation aided by pseudo-range measurements," *J. Dyn. Syst., Meas., Control*, vol. 139, no. 1, p. 011007, 2016.

[32] J. Chang, J. Zhou, A. Zolghadri, J. Cieslak, and Z. Guo, "A two-step approach for an enhanced quadrotor attitude estimation via IMU data," *IEEE Trans. Control Syst. Technol.*, vol. 26, no. 3, pp. 1140–1148, May 2018.

[33] W. Higgins, "A comparison of complementary and Kalman filtering," *IEEE Trans. Aerosp. Electron. Syst.*, vol. AES-11, no. 3, pp. 321–325, May 1975.

[34] J. L. Marins, X. Yun, E. R. Bachmann, R. B. McGhee, and M. J. Zyda, "An extended Kalman filter for quaternion-based orientation estimation using MARG sensors," in *Proc. IEEE/RSJ Int. Conf. Intell. Robots Syst. Expanding Societal Role Robot. Next Millennium*, vol. 4, Oct./Nov. 2001, pp. 2003–2011.

[35] M. Euston, P. Coote, R. Mahony, J. Kim, and T. Hamel, "A complementary filter for attitude estimation of a fixed-wing UAV," in *Proc. IEEE/RSJ Int. Conf. Intell. Robots Syst. (IROS)*, Sep. 2008, pp. 340–345.

[36] R. Mahony, T. Hamel, and J.-M. Pflimlin, "Nonlinear complementary filters on the special orthogonal group," *IEEE Trans. Autom. Control*, vol. 53, no. 5, pp. 1203–1218, Jun. 2008.

[37] S. O. H. Madgwick, A. J. L. Harrison, and R. Vaidyanathan, "Estimation of IMU and MARG orientation using a gradient descent algorithm," in *Proc. IEEE Int. Conf. Rehabil. Robot.*, Jun./Jul. 2011, pp. 1–7.

[38] Y. Tian, H. Wei, and J. Tan, "An adaptive-gain complementary filter for real-time human motion tracking with MARG sensors in free-living environments," *IEEE Trans. Neural Syst. Rehabil. Eng.*, vol. 21, no. 2, pp. 254–264, Mar. 2013.

[39] Y. Tian, W. R. Hamel, and J. Tan, "Accurate human navigation using wearable monocular visual and inertial sensors," *IEEE Trans. Instrum. Meas.*, vol. 63, no. 1, pp. 203–213, Jan. 2014.

[40] H. Fourati, N. Manamanni, L. Afilal, and Y. Handrich, "Complementary observer for body segments motion capturing by inertial and magnetic sensors," *IEEE/ASME Trans. Mechatronics*, vol. 19, no. 1, pp. 149–157, Feb. 2014.

[41] H. Fourati, N. Manamanni, L. Afilal, and Y. Handrich, "A nonlinear filtering approach for the attitude and dynamic body acceleration estimation based on inertial and magnetic sensors: Bio-logging application," *IEEE Sensors J.*, vol. 11, no. 1, pp. 233–244, Jan. 2011.

[42] G. Wahba, "A least squares estimate of satellite attitude," *SIAM Rev.*, vol. 7, no. 3, p. 409, 1965.

[43] F. L. Markley and D. Mortari, "How to estimate attitude from vector observations," *Adv. Astron. Sci.*, vol. 103, pp. 1979–1996, 2000.

[44] K. S. Arun, T. S. Huang, and S. D. Blostein, "Least-squares fitting of Two 3-D point sets," *IEEE Trans. Pattern Anal. Mach. Intell.*, vol. PAMI-9, no. 5, pp. 698–700, Sep. 1987.

[45] F. L. Markley, "Attitude determination using vector observations and the singular value decomposition," *J. Astron. Sci.*, vol. 36, no. 3, pp. 245–258, 1988.

[46] J. Wu, Z. Zhou, R. Li, L. Yang, and H. Fourati, "Attitude determination using a single sensor observation: Analytic quaternion solutions and property discussion," *IET Sci., Meas. Technol.*, vol. 11, no. 3, pp. 731–739, 2017.

[47] M. D. Shuster and S. D. Oh, "Three-axis attitude determination from vector observations," *J. Guid. Control, Dyn.*, vol. 4, no. 1, pp. 70–77, 1981.

[48] F. L. Markley, "Attitude determination using vector observations: A fast optimal matrix algorithm," *J. Astron. Sci.*, vol. 41, no. 2, pp. 261–280, 1993.

[49] J. Wu, Z. Zhou, B. Gao, R. Li, Y. Cheng, and H. Fourati, "Fast linear quaternion attitude estimator using vector observations," *IEEE Trans. Autom. Sci. Eng.*, vol. 15, no. 1, pp. 307–319, Jan. 2018.

[50] J. Wu, Z. Zhou, and M. Song. (Jul. 2018). "Convexity analysis of optimization framework of attitude determination from vector observations." [Online]. Available: https://arxiv.org/abs/1807.04931

[51] J. A. Farrell, *Aided Navigation: GPS With High Rate Sensors*. New York, NY, USA: McGraw-Hill, 2008.

[52] D. Titterton and J. L. Weston, *Strapdown Inertial Navigation Technology*, vol. 17. Edison, NJ, USA: IET, 2004.

[53] R. Mahony, T. Hamel, and J.-M. Pflimlin, "Complementary filter design on the special orthogonal group $SO(3)$," in *Proc. 44th IEEE Conf. Decis. Control, Eur. Control Conf. (CDC-ECC)*, vol. 1, Dec. 2005, pp. 1477–1484.

[54] D. Mortari, "ESOQ: A closed-form solution to the Wahba problem," *J. Astron. Sci.*, vol. 45, no. 2, pp. 195–204, 1997.

[55] M. Brown and D. G. Lowe, "Automatic panoramic image stitching using invariant features," *Int. J. Comput. Vis.*, vol. 74, no. 1, pp. 59–73, Aug. 2007.

[56] K. Mikolajczyk and C. Schmid, "A performance evaluation of local descriptors," *IEEE Trans. Pattern Anal. Mach. Intell.*, vol. 27, no. 10, pp. 1615–1630, Oct. 2005.

[57] H. Bay, A. Ess, T. Tuytelaars, and L. Van Gool, "Speeded-up robust features (SURF)," *Comput. Vis. Image Understand.*, vol. 110, no. 3, pp. 346–359, 2008.

[58] C. Ye, S. Hong, and A. Tamjidi, "6-DOF pose estimation of a robotic navigation aid by tracking visual and geometric features," *IEEE Trans. Autom. Sci. Eng.*, vol. 12, no. 4, pp. 1169–1180, Oct. 2015.

[59] D. Honegger, L. Meier, P. Tanskanen, and M. Pollefeys, "An open source and open hardware embedded metric optical flow CMOS camera for indoor and outdoor applications," in *Proc. IEEE Int. Conf. Robot. Autom.*, May 2013, pp. 1736–1741.

[60] Z. Wu, Y. Wu, X. Hu, and M. Wu, "Calibration of three-axis strapdown magnetometers using particle swarm optimization algorithm," in *Proc. IEEE Int. Symp. Robot. Sensors Environ. (ROSE)*, 2001, pp. 160–165.

[61] Z. Zhang, "A flexible new technique for camera calibration," *IEEE Trans. Pattern Anal. Mach. Intell.*, vol. 22, no. 11, pp. 1330–1334, Nov. 2000.

[62] S. Brás, R. Cunha, J. F. Vasconcelos, C. Silvestre, and P. Oliveira, "A nonlinear attitude observer based on active vision and inertial measurements," *IEEE Trans. Robot.*, vol. 27, no. 4, pp. 664–677, Aug. 2011.

[63] A. Geiger, P. Lenz, C. Stiller, and R. Urtasun, "Vision meets robotics: The KITTI dataset," *Int. J. Robot. Res.*, vol. 32, no. 11, pp. 1231–1237, 2013.

[64] Z. Zhou, J. Wu, J. Wang, and H. Fourati, "Optimal, recursive and sub-optimal linear solutions to attitude determination from vector observations for GNSS/accelerometer/magnetometer orientation measurement," *Remote Sens.*, vol. 10, no. 3, pp. 377–405, 2018.

Jin Wu (M'17) was born in Zhengjiang, Jiangsu, China, in May 1994. He received the B.S. degree in automation engineering from the University of Electronic Science and Technology of China, Chengdu, China.

He is currently a Research Assistant with the School of Aeronautics and Astronautics, University of Electronic Science and Technology of China. He has published more than 20 technical papers on academic journals and conference proceedings, e.g., IEEE Transactions, IEEE Journals, IET Journals, and so on. His research interests include inertial navigation, optimal filtering, control theory, and robot vision.

Zebo Zhou received the B.Sc. and M.Sc. degrees from the School of Geodesy and Geomatics, Wuhan University, Wuhan, China, in 2004 and 2006, respectively, and the Ph.D. degree from the College of Surveying and Geo-Informatics, Tongji University, Shanghai, China, in 2009.

In 2009 and 2015, he was a Visiting Fellow with the Surveying and Geospatial Engineering Group, School of Civil and Environmental Engineering, University of New South Wales, Sydney, NSW, Australia. He is currently an Associate Professor with the School of Aeronautics and Astronautics, University of Electronic Science and Technology of China, Chengdu, China. His research interests include GNSS navigation and positioning, GNSS/INS integrated navigation, and multisensor fusion.

Hassen Fourati received the B.E. degree in electrical engineering from the National Engineering School of Sfax, Sfax, Tunisia, in 2006, the master's degree in automated systems and control from the University Claude Bernard, Lyon, France, in 2007, and the Ph.D. degree in automatic control from the University of Strasbourg, Strasbourg, France, in 2010.

He is currently an Associate Professor with the Department of Electrical Engineering and Computer Science, University Grenoble Alpes, Grenoble, France, and a member of the Networked Controlled Systems Team, affiliated to the Automatic Control Department, GIPSA-Lab, Grenoble, France. His research interests include nonlinear filtering and estimation and multisensor fusion with applications in navigation, robotics, and traffic management.

Rui Li (M'10) received the Ph.D. degree in control science and engineering from the Harbin Institute of Technology, Harbin, China, in 2008.

She was a Visiting Research Associate with the Department of Applied Mathematics, The Hong Kong Polytechnic University, Hong Kong, and the Department of Mathematics and Statistics, Curtin University of Technology, Perth, WA, Australia. In 2008, she joined the University of Electronic Science and Technology of China, Chengdu, China, where she is currently an Associate Professor with the School of Automation. From September 2011 to September 2012, she was a Visiting Scholar with the Department of Electrical Engineering, University of California at Riverside, Riverside, CA, USA. Her research interests include optimization theory and optimal control, nonlinear control, multiagent systems, and aircraft control.

Ming Liu (S'12–M'12–SM'18) received the B.A. degree in automation from Tongji University, Shanghai, China, in 2005, the master's degree from Tongji University, and the Ph.D. degree from the Department of Mechanical Engineering and Process Engineering, ETH Zurich, Zurich, Switzerland, in 2013.

He was a Visiting Scholar with Erlangen Nurnberg University, Erlangen, Germany, and the Fraunhofer Institute IISB, Erlangen. He is currently an Assistant Professor with the Department of Electronic and Computer Engineering, The Hong Kong University of Science and Technology, Hong Kong. His current research interests include autonomous mapping, visual navigation, topological mapping, and environment modeling.

Prof. Liu was a recipient of the Best Student Paper Award from the IEEE MFI 2012, the Best Paper in Information Award from the IEEE ICIA 2013, the Best RoboCup Paper from the IEEE IROS 2013, and twice the Winning Prize of the Chunhui-Cup Innovation Contest. He is currently on the Editorial Board of IEEE ROBOTICS AND AUTOMATION LETTERS.